ENERGY, ENVIRONMENT & STORAGE

AN INTERNATIONAL JOURNAL

Volume-3
Issue-2
May, 2023
ISSN: 2791-6197

Editor in Chief
Dr. Selahaddin Orhan AKANSU

ENERGY, ENVIRONMENT AND STORAGE

EES JOURNAL

Founded and Published by Erciyes Energy Association

Energy, Environment and Storage Journal is indexed in Crossref

Printed in Turkey

ISSN-2791-6197

EES- EDITORIAL BOARD

BOARD MEMBER

VOLUME 3, ISSUE 2, REVIEWER BOARD

Dr. Ali Tor

Dr. Feza Can

Dr. Kemal Doğan

Dr. M. Ilhan Ilhak

Dr. Rasit Atelge

Dr. Mahmut Caner Acar

Dr. Altuğ Karabey

Dr. Fulya Pelin Cengizoğlu

Dr. Srinivasarao Naik B

Dr. Mustafa Yasin Gökaslan

Dr. Yusuf Tekin

Dr. Mehmet Seyhan

Dr. Nora Salina

Dr. Duygu Uysal

EDITORIAL OFFICE

AIM AND SCOPE

Energy, Environment and Storage papers consider the prospects of energy technologies, environment, materials, process control and industrial systems. The Energy, Environment and Storage will be published 3 times per year.

Contributions describe novel and significant applications to the fields of:

- Hydrogen Fuels
- Hydrogen and Fuel Cell
- Hydrogen Economic
- Biomass
- Solar PV Technology
- Solar Thermal Applications
- Wind Energy
- Materials for Energy
- Drones and Energy Applications
- Nuclear Energy and Applications
- Hydro Power
- Fuel Technologies (CNG, LNG, LPG, Diesel, Gasoline, Ethanol, etc.)
- Numerical Modelling
- Energy Storage and Systems
- Battery Technologies
- Energy Management
- Heat and Mass Transfer
- Aerodynamics
- Aerospace and Energy Applications
- Combustion
- Electric Vehicle Transportation
- Off-grid Energy Systems
- Environment Management
- Air Pollution
- Water and Wastewater Pollution
- Water and Wastewater Management
- Waste Management
- Global Warming and Climate Change
- Environmental Ecosystem
- Environmental System Modelling and Optimization
- Ecological Applications or Conservation

VOLUME 3, ISSUE 2

MAY 2023

CONTENTS

Energy, Environment and Storage

Journal Homepage: www.enenstrg.com

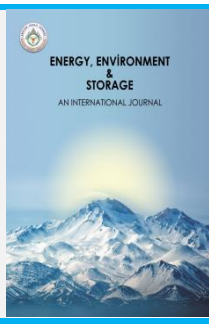

Evaluation of Conducting Properties of Biopolymer Electrolyte K-Carrageenan with The Effect of Three Different Ammonium Salts

M. Nithya[1]

[1]*Department of Physics, The SFR College for Women, Sivakasi. ORCID: 0000-0003-3605-6236*

ABSTRACT. In the present work kappa-carrageenan (KC) with different ammonium salts NH_4Cl, NH_4Br, and NH_4I membrane were successfully synthesized by the solution casting technique. The prepared eco-friendly membrane is subjected to ionic conductivity study, XRD study, transference number studies, and then it's compared. The ionic conductivity value for KC with 200 mg NH_4Cl is 1.81×10^{-4} S/cm, KC with 300 mg NH_4Br is 2.80×10^{-3} S/cm, KC with 400 mg NH_4I is 5.88×10^{-5} S/cm. Among all the three, combinations the KC with 300 mg NH_4Br gives high ionic conductivity. From the X-Ray Diffraction pattern, KC-NH_4Cl incorporation greatly enriched the amorphous region. All the three membranes transference numbers are very close to unity. Among all the three combinations, KC with 300 mg NH_4Br is the best combination for the application of fuel cell battery.

Keywords: kappa-carrageenan, Ammonium salts, Electrolytic conductivity, Ionic Transport.

Article History: Received: 31.01.2023; Accepted:05.02.2023; Available Online: 26.05.2023
Doi: https://doi.org/10.52924/YTMK4887

1. INTRODUCTION

The conductivity of a material is the major property of electrical appliances. The conductivity of the material is different for different materials. Production of electricity in the material depends on the dissolved impurities in the material. Depending upon the suspended ions the electrical charge is transferred in the material. Based on conductivity and resistivity, the conducting material is segregated into two main categories. The first one is the highest conductivity or lowest resistivity materials and the second one is the lowest conductivity or highest conductivity materials. In the field of electrical engineering applications, both the highest conducting materials and the lowest conducting materials play a vital role. The low conducting materials like carbon, tungsten are useful to fabricate the heating elements. The material of low resistivity and high conductivity is useful for an electrical machine, transmission, and distribution of electrical energy. Here our aim is to find the highest conducting material for energy-saving devices. The Highest conducting materials have the properties of the lowest possible resistance, the highest possible conductivity, good mechanical strength, stability, corrosion-free, low cost, long life, and a high elasticity [1, 2, 3]. The belongings of conducting material are varying for various purposes. The present work is to find a flexible, high conducting solid biopolymer. Because of the applications of the bio-polymer membranes in the fields of electronics, fuel cells, solar cells, batteries are increasing day by day. Compared to metal like silver, gold, and aluminum conductivity, polymers have low electrical conductivity reported by the researches in 1970 [4]. Nowadays the conductivity of polymer is increased the best selection of polymers and added impurities [5, 6, 7]. Kappa carrageenan solid polymer electrolytes [SPE] have a great attention in many electrolyte applications due to several good advantageous properties like ease of fabrication, flexibility in nature, cost effectiveness, good mechanical stability, and safety in use. To reduce environmental pollution, bio-based polymers are developed as electrolytes. It is one of the primary resources for recycling energy [8]. From the literature survey, we found a conductivity value for pure Kappa carrageenan of 6.76×10^{-6} S/cm at room temperature [1]. The selection of dopant is another goal to reach the highest conducting flexible biopolymer. We have selected a proton-conducting ammonium salts to achieve the highest conducting electrolyte. As we expected, prepared biopolymer conductivity increased [9].

In this present work, we have synthesized the biopolymer membrane by the choice of kappa carrageenan with different kinds of ammonium salts (NH_4Cl, NH_4Br, and NH_4I) [5].

*Corresponding author: nina07.muma@gmail.com

2. MATERIALS AND METHODS

2.1. Chemicals

Chemicals selected for this work are the biopolymer kappa-carrageenan (KC) [6] and NH_4Cl, NH_4Br, and NH_4I, which were purchased from TCI Chemicals, Coimbatore, Tamil Nadu.

2.2. Biopolymer Electrolyte Preparation

Biopolymer electrolytes were prepared by the solution casting method. The solution is prepared by using water as a solvent. First, prepare a fixed amount (1 g) of kappa carrageenan solution and different concentrations (200 mg, 300 mg, 400 mg) of ammonium salt (NH_4Cl, NH_4Br, NH_4I) solutions. Now mix 1 gm KC with 200 mg solutions and allow them to stir continuously without forming any bubbles. Similarly prepare the solutions for different concentrations. The solutions were prepared at room temperature. Then the solutions are transferred into petri dishes, which are then kept inside the oven to maintain the temperature range of 45°C. After all this processing, transparent and flexible biopolymer membranes were obtained.

2.3. XRD

The materials phase transformation from crystal to polymer is studied by PANalytical X' pert Pro powder X'celerator Diffractometer instrument. The membranes were measured in the range of 10 to 80 degrees in 2θ.

2.4. Electrolytic conductivity:

The electrolytic conductivity of three different ammonium salts in kappa-carrageenan was analyzed by the formula of

$$\sigma = t/AR_b \text{ (S/cm)}$$

Where't' and 'A' are the thickness and area of the polymer electrolyte film respectively. R_b is the bulk resistance of the polymer membrane [10].

2.5. Ionic Transport Analysis

Ionic transference numbers are calculated by the below-mentioned equation, and it is determined by the Wagner procedure [11].

$$T_{ion} = (I_{initial} - I_{final})/ I_{initial}$$

In this procedure fixed DC voltage of 1.8 V is applied across the cell.

3. STUDIES AND ANALYSIS

3.1. XRD Discussion

The intensity of the peaks in pure Kappa carrageenan decreases when we add 200mg NH_4Cl. And the beaks are shifted to wide-angle value [7] by the addition of 300mg NH_4Br and 400mg NH_4I salts. Figure 1 shows the amorphous range of prepared biopolymers. The interaction between used salts and biopolymers results in a merely increased amorphous nature from pure to doped electrolyte. The maximum amorphous nature is observed in 1 g of KC and 200 mg of NH_4Cl-doped electrolyte. The broadening of the spectrum at 300mg NH_4Br and 400mg NH_4I salts. This is because the biopolymer was unable to accommodate the used salt, which leads to the recombination of the ions [9].

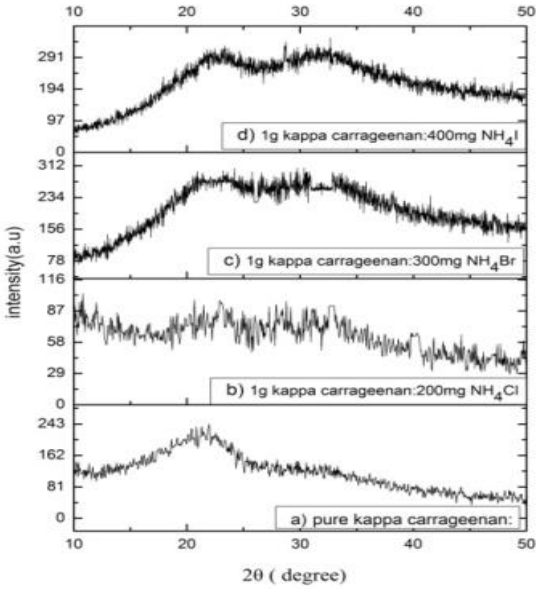

Fig.1. Amorphous nature of Pure and ammonium salts doped membrane

Compared to pure KC, 200 mg NH_4Cl, 300 mg NH_4Br, 400 mg NH_4I added electrolytes are having a more amorphous phase which may enhance the ionic conductivity of the biopolymer electrolyte [7]. From the XRD analysis, we find the selected highest conducting biopolymer electrolytes are having a polymer nature, and it has better ionic conductivity.

3.2. Electrolytic conductivity

The Cole-Cole plots of the pure kappa-carrageenan and ammonium salts doped kappa-carrageenan biopolymer electrolytes are shown in figure 2.

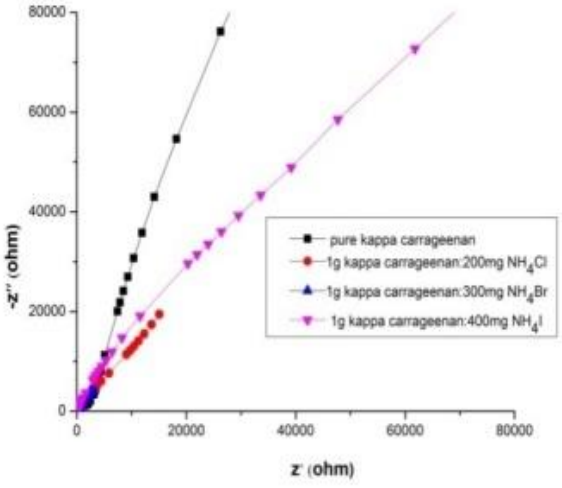

Fig.2. Cole-Cole plots of the pure kappa-carrageenan and ammonium salts doped membrane.

The ionic conductivity value for 1gm kappa with 200 mg NH_4Cl is 1.81×10^{-4} S/cm,1gm kappa with 300 mg NH_4Br is 2.80×10^{-3}S/cm, 1gm kappa with 400 mg NH_4I is 5.88×10^{-5} S/cm. 200 mg of NH_4Cl, 300mg of NH_4Br, and 400mg of NH_4I salt concentrations are well incorporate with the 1 g of KC. Beyond the addition of 200 mg of NH_4Cl, 300mg of NH_4Br, and 400mg of NH_4I salt concentrations, the Cole–Cole plot indicates the resistive component exits in the polymer electrolyte and is corresponding to the mobile ion being less in the polymer [12]. Among all the three, combinations the 1gm K-carrageenan with 300 mg NH_4Br gives the high ionic conductivity in the order of 2.80×10^{-3} S/cm. Figure 3 drawn for the conductivity of prepared biopolymer membranes with different concentrations of ammonium salts. Calculated ionic conductivity as a function of ammonium salts.

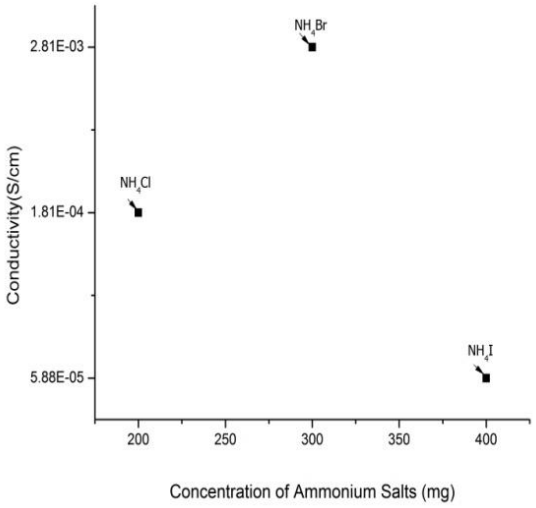

Fig.3. Variation of conductivity as a function of ammonium salts.

3.3. Ionic Transport Analysis

The initial polarization currents of all three membranes are decreases with time due to the depletion of the ionic species in the electrolyte and finally, it is constant in the fully depleted situation. This is because the ionic current through an ion-blocking electrode falls rapidly with time. The initial current for the present study of 1gm K-carrageenan with 200 mg NH_4Cl, 300 mg NH_4Br, and 400 mg NH_4I are 110 µA, 230 µA, and 170µA respectively. Calculated transference numbers are very close to unity. The Polarization verses time graph is shown in figure 4.

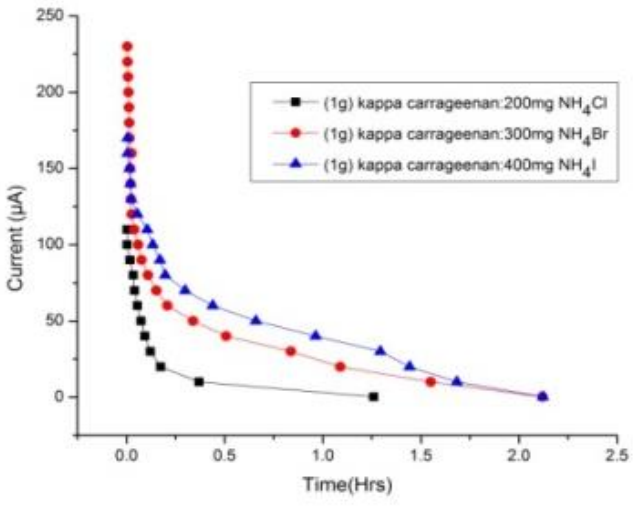

Fig. 4. Polarization current verses time for prepared bio polymer Membrane.

4. CONCLUSION

Kappa-carrageenan (KC) with different ammonium salts NH_4Cl, NH_4Br, and NH_4I membrane were successfully synthesized by the solution casting technique.

From the conductivity studies, the maximum ionic conductivity of prepared biopolymer film was 2.80×10^{-3} S/cm, it is achieved for the membrane doped with 300 mg NH_4Br salt concentration. Due to the better conductivity and mobility, this biodegradable kappa carrageenan based flexible solid electrolytes in association with conducting salts were used in different bio polymer battery [13] assemblies.

REFERENCES

[1] M.Nithya, M. Alagar, B. Sundaresan. 10.1016/j.matlet.2019.127295.

[2] J.B. Goodenoough, K.S Park, J.Am. Chem. Soc.135 (2013) 1167-1176 .(2004) Census 2002. National Report, Central Statistical Office, Harare

[3] D.Y. Park, D.Y. Park, Y. Lan, Y.S Lim, M.S.Kim, J.Ind. Eng. Chem. 15 (2009) 588-594.

[4] K.P. Radha, S. Selvasekarapandian, S.Karthikeyan, M.Hemalatha, C.Sanjeeviraja, D. Vinoth Pandi. Int. J. Electroactive Mater. 2 (2012) xx-yy.

[5] Khalid Mahmood Zia Shazia Tabasum Muhammad Nasif Neelam Sultan Nosheen Aslam Aqdas Noreen. 10.1016/j.ijbiomac.2016.11.095.

[6] V. Moniha, M. Alagar, S. Selvasekarapandian, B. Sund aresan, R. Hemalatha, G. Boopathi J. Solid State Electrochem. 22 (10) (2018), pp. 1-15

[7] N.K. Zainuddin, A.S. Samsudin. Materials Today Communications 14 (2018) 199-209.

[8] S Rudhziah, NAC Apandi, RHY Subban, NS Mohamed. 2018 *Sci. Lett.* **12**, 45–52.

[9] M.Nithya, M. Alagar, B. Sundaresan. J. Int. Sci. Technol. 2020, 8(1), 1-5

[10] V. Moniha, M. Alagar, S. Selvasekarapandian, B. Sundaresan, G. Boopathi, G. Boopathi. Journal or Non – Crystalline Solids 481 (2018) 424-434

[11] P. Sangeetha, T.M.Selvakumari, S. Selvasekarapandian, S.R.Srikumar, R.Manjuladevi, M.Mahalakshmi. Ionics 10.1007/s11581-019-03193-0

[12] P.Perumal, S. Selvasekarapandian, K.P.Abhilash, P.Sivaraj, R.Hemalatha, P.Christopher selvin. 10.1016/j.vacuum.2018.10.043

[13] G. Boopothi, S. Pugalendhi, S. Selvasekarapandian, M. Premalatha, S. Monisha, G. Aristatil (2016) Ionics 23:2781–2790

Research Article *Energy, Environment and Storage* (2023)03-02:45-51

Energy, Environment and Storage

Journal Homepage: www.enenstrg.com

Determination of a New Performance Indicator for the Assessment of Stand-Alone PV System

Francis-Daniel MENGA[1*], Jorel landry OWONA[2], Oumarou DJOUBAIROU OUMAROU[3]

[1] *National Committee for Development of Technologies (NCDT), Yaoundé, Cameroon, ORCID: 0000-0002-6165-0010*
[2] *National Committee for Development of Technologies (NCDT), Yaoundé, Cameroon, ORCID: 0009-0005-9245-2585*
[3] *National Committee for Development of Technologies (NCDT), Yaoundé, Cameroon, ORCID: 0009-0002-9058-1920*

ABSTRACT. The use of stand-alone PV systems (*SAPV*) must be efficient and profitable for a better integration of solar energy in the global energy mix. However, the performance indicators that allow the evaluation of *SAPV* systems do not clearly inform us about the actual level of use of their sized and installed capacity. This article aims to determine a new performance indicator, called the theoretical power factor (*TPF*) by an original method based on the modelling of the *SAPV* system in the form of a matrix equation. The resolution of this matrix equation, makes it possible to bring out the reactive energy of the system during operation. A case study is presented and scenario I represents the case where the main elements are all assumed to operate at their rated capacity. scenario II represents the case were the rated capacity of storage system is reduced of 40%, scenario III represents the case were the rated current capacity of charge controller is reduced of 40%, and finally scenario IV represents the case were the rated power capacity of inverter is also reduced of 40%. The results obtained after implementation in the Spyder environment (python 5.1) show the effectiveness of *TPF* in the performance evaluation of *SAPV* systems. And also show how the *TPF* is substantially related to the capacity of each main element of the system. This being proved by the results obtained after the simulation of the four scenarios mentioned above. One can observe an increase in *TPF* of 0.1% in Scenario II during the period of low irradiance, and no change in *TPF* for the other scenarios in the same period. During the period of high irradiance, an increase in *TPF* of 17.9% is observed in scenario II and a decrease in *TPF* of 15.4% and 1.2% respectively in scenarios III and IV.

Keywords: Stand-Alone PV system, Performance indicators, Performance Ratio, Reactive energy, Theoretical power factor, Matrix model

Article History: Received: 06.02.2023; Accepted: 16.02.2023; Available Online: 26.05.2023
Doi: https://doi.org/10.52924/QBMK2848

1. INTRODUCTION

Solar photovoltaic energy is a solution to the energy deficit observed in several developing countries. It is also a source of energy that helps to reduce the pollution caused by the use of fossil fuels. Solar energy conversion systems, also known as PV systems, are becoming increasingly popular in sub-Saharan Africa. Electricity from solar PV contribute at 3% of global electricity generation in the world and it is now the third-largest renewable electricity technology after hydro power and onshore wind [1]. Depending on the installation site and the intermittent nature of the solar energy source, these systems can be connected to an electrical distribution network or be associated with other energy sources (wind, diesel, etc.) to form hybrid sources. Or they can be combined with batteries to store electrical energy and form autonomous systems [2]. The choice of a PV configuration is usually based on technical, economic, social, environmental and political/legal criteria. In remote rural areas and some urban areas in sub-Saharan Africa, the choice is much more towards stand-alone PV systems with storage.

Stand-alone PV systems (SAPV) require good sizing. There are several sizing methods as presented in the articles [3], [4]. Due to the randomness of the solar energy source and the load profile, the reliability of stand-alone PV systems is questionable, regardless of the design method used. In the literature, several criteria for the reliability of PV systems can be distinguished [5].

The intermittency of the solar energy source, the variation in the load profile and the difficulty in obtaining certain technical and social environment data from the site where the system is to be installed, means that no sizing method is completely reliable. It is difficult to accurately design a PV system. In general, the mode of operation for which the system is designed is not always real (e.g., the power demand taken into account in the design calculations is variable in reality and can sometimes exceed the estimated power). It is therefore important to study the performance of a stand-alone PV system that has been designed.

*Corresponding author: danielmenga6@gmail.com

To assess the performance of SAPV system there are several types of indicators [5]–[8]. Among these indicators, the performance ratio (PR) is one of the most significant for evaluating the efficiency of the PV system. Specifically, the performance ratio is the ratio of the actual and theoretically possible energy outputs. It tells us about the electrical energy converted by PV solar panels and which is actually used by the load. And it is largely independent of the orientation of a PV plant and the incident solar irradiation on the PV plant. The performance ratio is a parameter that emerges in several studies concerning the performance evaluation of stand-alone and grid-connected PV systems [9]– [12].

However, the calculation of the performance ratio requires, for a given time, the actual consumption measurements of the load [13], [14]. This implies measurements on operational PV systems. such a performance ratio evaluation of a PV system would certainly be realistic but very expensive for a post-installation performance evaluation. there are also sizing software packages such as PVsyst, INSEL, TRNSYS, PVSOL, SOLARPRO [10] which can evaluate the performance ratio during the sizing of the PV system. But the software takes into account the estimated load consumption data. this makes the performance ratio calculation approximate and unrealistic for systems without a demand side management system.

The main problem with the performance ratio is that the size of the battery, charge controller and inverter does not clearly influence performance ratio value. This hiding the fact that the performance ratio can be caused by poor system sizing and poor storage management. The same performance ratio value can be obtained by two SAPV systems with different size of inverter, battery storage and charge controller.

In this work, the performance ratio of a stand-alone PV system is predicted just from the knowledge of the size of its components, the meteorological data and the electrical consumption data. The size of the different components of the system can therefore be varied to study their influence on the performances indicators (the conventional one and the new one). So, our objective is to determine a new reliability indicator thanks to an original method of calculation. This new reliability indicator is named the theoretical power factor (TPF). Which is obtained by considering the set (Charge Controller-battery-Inverter-Load) as a whole electrical receiver. and as with any electrical receiver its power factor can be determined. Two determine TPF an original method is developed and consists in modelling the PV Stand-Alone System as a matrix equation whose solution allows to calculate the TPF. The TPF is considered more as a new reliability indicator of the PV stand-alone system sized. In the same way as the Loss of Power Supply Probability (LPSP), the Loss of Load Probability (LOLP or LLP) and many others that each carry a specific information [4], [13].

To achieve our goal, the SAPV system will first be described. Then, an energy model of the SAPV system in matrix equation form, for the determination of the new reliability indicator will be developed. And the TPF will be calculated according the case study which will be presented. Finally, the results obtained by the implementation and simulation in an integrated development environment (SPYDER) will be presented before the conclusion.

2. MATERIALS AND METHODS

2.1 Description of the Stand-Alone PV system studied

The main components of the PV/Battery system are: The PV generator, the charge regulator (or charge controller), the batteries and the inverter. The PV generator produces the electrical energy for the load consumption. Batteries storage are used to store the excess electrical energy produced by the PV generator during the day. This energy is then consumed by the load at the night or when the generated energy by the solar panels is not enough (low sunlight) to respond to the load demand. The role of the charge controller is to ensure that the battery charging and discharging processes, are carried out, so that they are always in the correct operating conditions. It also permits to maximize the power of solar panels. The role of the inverter is to convert direct current (DC) into alternating current (AC). Since photovoltaic solar panels generate direct electricity current, and most of devices used in houses or in professional offices work with alternating current, this component is therefore for a particular importance in photovoltaic systems. Schematic representation of the studied system is given in Fig.1.

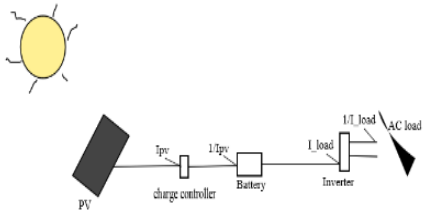

Fig. 1. Stand-Alone PV system

2.2 Performance Ratio PR

The performance ratio is a measure of the quality of a PV plant that is independent of location and it therefore often described as a quality factor. The performance ratio (PR) is stated as percent and describes the relationship between the actual and theoretical energy outputs of the PV plant. The closer the PR value determined for a PV plant approaches 100 %, the more efficiently the respective PV plant is operating. In real life, a value of 100 % cannot be achieved, as unavoidable losses always arise with the operation of the PV plant (e.g., thermal loss due to heating of the PV modules). High-performance PV plants can however reach a performance ratio of up to 80 %.
The Performance Ratio can be calculated either manually or automatically by software such as PVsyst. the formula of the PR is written [11]:

$$PR = \frac{E_{actual}}{E_{nominal}} = \frac{E_{actual}}{G_{period} * \eta_{STC} * A} \quad (1)$$

where $\boldsymbol{E_{actual}}$ is the actual reading of PV plant output in kW h, which is the energy consumed by the load side at the end of analysis period, $\boldsymbol{E_{nominal}}$ is the calculated nominal PV plant output, $\boldsymbol{G_{period}}$ is the solar radiation incident at the end analysis period, $\boldsymbol{A}$ the entire module

surface, and η_{STC} is the nominal efficiency of the PV module under Standard Test Conditions) STC.

2.3 New performance indicator determination

The reliability indicator proposed in this work allows to determine over a given time the theoretical power factor (TPF) which is an average percentage of use of the SAPV system supplying a non-exhaustive and variable load. This indicator is determined through the matrix modelling of the SAPV system.

2.3.1 Modelling of SAPV system sized

The SAPV system is basically consists of PV modules, a charge controller or regulator, a storage device and inverter for AC appliances.
The model proposed here is developed by considering some of the following assumptions:

- The sized SAPV system can work perfectly without failure;
- The internal physical properties of each element of the system are neglected;
- The data considered are hourly average values.

Fig.1 shows the energy transfer from solar radiation to the load, through the components of the SAPV system. The model represents in the matrix equation form (A.X = B), the energy transfer from the PV generator to the load through the battery. Where A is a matrix of dimension *m* × *n* representing energy flow between each characteristic component of SAPV system and B is the column vector of dimension n representing the Energy and voltage state of each characteristic element during its operation. Solving this equation informs us about the balance between the energy generated by the system and the energy consumed by the load. It also informs us about the size of the system. Indeed, due to the variations in load and weather conditions, it is rare that the energy generated is equal to the energy consumed. Most of the time the system operates in an energy imbalance between supply and demand. It is in this latter case that the size of system is important.

Determination of the parameters of matrix A

The parameters of matrix A are determined according to an original logic, quite similar to the one used to determine the adjacency matrix in the graph theory [15]. By considering our SAPV system as an oriented graph in which the energy transit elements (PV generator, Charge Controller, battery, inverter and load) are nodes, the value of each edge connecting two nodes is determined by considering the following rules:

• When electrical energy flows from an active dipole to a passive dipole, the value of the edge is equivalent to the maximum current capable of flowing through the link between these two dipoles;

• And when the electrical energy flows from a passive dipole to an active dipole, the value of the edge is equivalent to the inverse of the maximum current capable of flowing through the link between these two dipoles.

So, one can write this:

$$A=\begin{bmatrix} 1 & I_{ccN} & 0 & 0 & 0 \\ 0 & 1 & 1/I_{ccN} & 0 & 0 \\ 0 & 0 & 1 & I_{invN} & 0 \\ 0 & 0 & 0 & 1 & 1/I_{invN} \\ 0 & 0 & 0 & 0 & 1 \end{bmatrix} \quad (2)$$

where I_{ccN} is the nominal current which can flow through the charge controller to the battery system and I_{invN} is the nominal current of inverter which can flow through the inverter to the load.

Determination of the parameters of vector B

B(t) is the column vector that provides information on the status of the characteristic parameters of each element of the SAPV system at each time *t* of a given period *T*. The PV generator, the battery and the load are characterized by their Energy level, while the charge controller and the inverter are characterized by their terminal voltage level. *B* vector at the specific time is given by this:

$$B=\begin{bmatrix} E_{pv} \\ V_{cc} \\ E_{bat} \\ V_{inv} \\ E_{load} \end{bmatrix} \quad (3)$$

Where E_{pv} is effective energy converted into electrical energy by the solar PV. It is written:

$$E_{pv} = G * A_{pv} * \eta_{pv} \quad (4)$$

G is the hourly global irradiance in (Wh/m^2). A_{pv} is the total array surface in (m^2) and η_{pv} is the photovoltaic panel efficiency. V_{cc} and V_{inv} are respectively the terminal voltage of charge controller and terminal voltage of inverter. E_{bat} is energy battery which is either stored or restored. It is given by this following equation:

$$E_{bat} = C_{bat} * V_{bat} \quad (5)$$

The instantaneous storage capacity of the batteries C_{bat} is given by:

$$C_{bat}(t) = C_{bat}(t-1) + (I_{PV} * \Delta t - I_{load} * \Delta t) \quad (6)$$

V_{bat} is the terminal voltage of batteries storage system.

I_{PV} is the PV current delivered by the generator for each time interval (Δt), here Δt =1 h.
This current is determined following this equation:

$$I_{PV} = \frac{E_{pv}}{V_{cc} * \Delta t} \quad (7)$$

I_{load} is current of load for each time interval. Determined by:

$$I_{load} = \frac{E_{load}}{V_{inv}*\Delta t} \quad (8)$$

With E_{load} which is the energy need at load for one hour.

2.3.2 Theoretical Power Factor (TPF)

TPF is the proposed performance indicator. Theoretical because there are some assumptions took into account for its determination. Cleary, it is an average percentage of system usage determined by solving the matrix equation $AX = B$ each time interval. The vector X is a solution obtained each time interval and whose first term X_1 corresponds to a reactive energy. This reactive energy is composed of the electrical energy produced by the PV generator that has not been consumed or stored, the energy difference between the maximum energy capacity of the charge controller and the energy that actually flows through it in each time interval and finally the energy difference between the maximum energy capacity of the inverter and the energy consumed by the load at a given time. these reactive energy components are losses related to the size of the system elements and the management method of the storage system. The following equation gives the TPF.

$$TPF = \frac{\sum_{i=1}^{nh} \sqrt{1-\left(\frac{X_1[i]}{P_{pv,Peak}*\Delta t}\right)^2}}{nh} \quad (9)$$

$$TPF = \begin{cases} 0 \;\; if \;\; X_1[i] \geq \;\; P_{pv,Peak} * \Delta t \\ 1 \qquad\quad if \qquad X_1[i] \;=\; 0 \end{cases} \quad (10)$$

where $P_{pv,Peak}$ is a nominal power of PV generator and nh is a number of the total hours of the given period.

It is important to note that, concerning the performance PV plant assessment, this performance indicator does not appear in the literature and especially not among the indicators proposed by the IEA PVPS Task 2 [7], [8].

2.4 Implementation data and strategy

The meteorological data (irradiance), constituting the important input parameters of the PV generator, is downloaded from the Helioclim-3 Archive Database of Solar Irradiation V5 (derived from satellite data) and meteorological data (MERRA-2/NASA and GFS/NCEP) for two periods of year (2020-02-01 to 2021-02-09 and 2020-08-08 to 2021-08-15) and for precise location of the Yaoundé, Cameroon. The energy demand is also a key input parameter for the simulation of the system. Fig. 2 shows the daily energy demand.

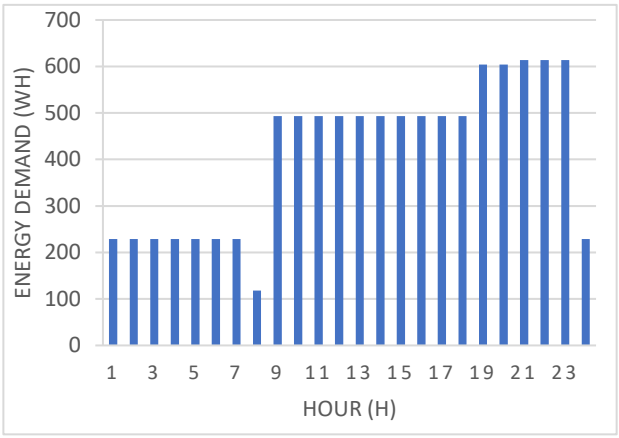

Fig. 2. Daily energy demand

In the defined operational strategy, the PV power production is determined for each time interval corresponding to the given meteorological data. The description of the strategy of the studied system, is given in Fig. 3.

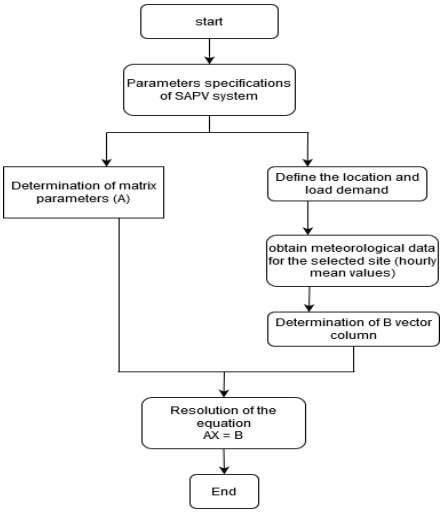

Fig. 3 Diagram of SAPV model implementation

Table 1. Parameters used for simulation

Designation	Value
Type of system	Stand-alone system
Nominal power of PV plant	3500 Wp
Nominal capacity of battery	1260 Ah
Total surface of PV plant	19.9 m^2
Allowable depth of discharge of batteries	80 %
Nominal power of inverter	635 W
Maximum current of charge controller	93 A
Batteries bank Voltage	26 V
Efficiency of conversion PV	15 %

To analyse the influence of the size of each element of the SAPV system. From the second scenario to the fourth scenario the size of an element (charge controller, battery and inverter) of the system will be reduced from 100% to 60% of their initial size as shown in table 2. The value

60% is a randomly chosen coefficient that has no particular meaning but will allow us to observe and analyse the values of the different performance indicators.

Table 2. simulation scenarios

	Scenarios			
	I	II	III	IV
Surface of PV plant (%)	100	100	100	100
Current of charge controller (%)	100	100	60	100
Capacity of Battery (%)	100	60	100	100
Capacity of inverter (%)	100	100	100	60

3. RESULTS AND DISCUSSION

The results obtained here after implementation and simulation in the Spyder environment (Python 5.1) allow, over a period of time, an analysis of the evolution of the reactive energy of the SAPV system in operation. Remembering that the reactive energy of the system, which is noted X1, is the first term of the solution vector X of the matrix equation of our system. The results obtained allow also to compare the performance indicators (Performance Ratio and Theoretical Power Factor) of the SAPV system between to different period of a year. One can finally observe the influence of the size of component systems on the performance indicators.

3.1 Analysis of the reactive energy evolution of the SAPV system during a period

Fig. 4 shows the evolution of the reactive energy and the energy produced by the PV generator during the August period. It can be seen that the reactive energy is positive and is very high. This reactive energy is more important during periods of low sunshine than during periods of high sunshine. This development indicates that the overall capacity of the SAPV system is low. This will be determined by the proposed performance indicator, the theoretical power factor (TPF) in Table 3. The period of August is generally a period of low irradiance in Yaoundé, Cameroon. This is most easily explained by the fact that the irradiance is low and the SAPV system is used below its nominal performance.

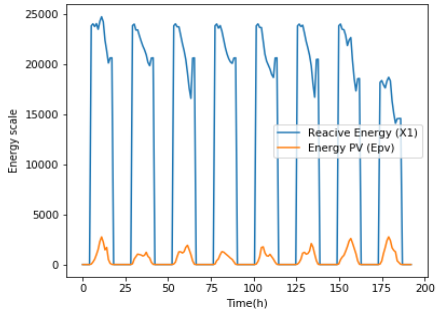

Fig. 4. Profile of reactive energy and PV energy produced

3.2 Comparison of the performance indicators for SAPV system according to two analysis periods

Simulation of scenario I is made for the nominal capacity of each component of SAPV system. Table 3 shows that, during periods of high irradiance the performance ratio (PR) decreases and the theoretical power factor (TPF) increases compared to the periods of low irradiance. a fairly predictable result because when the irradiance increases the energy converted by the PV panels also increases while the energy consumed remains the same. then the PR decreases.

However, when this PV energy increases the current also increases in the charge controller and the storage system is charging faster. This will be checked looking the final state of charge (SOC) of the battery which is 38% for the period of low irradiation against 84% in the period of high irradiation.

Table 3 Comparison of *PR* and *TPF* in nominal capacity of SAPV system

Performance Indicators	**Periods**	
	August period (Low irradiance)	February period (High irradiance)
PR	0.757	0.674
TPF	0.458	0.612

3.3 Influence of storage system capacity on the performance indicators

Simulation of scenario II is made to see the influence of the capacity of storage system on the performance indicators. One can observe from table 4 that, the capacity of the storage system does not influence the performance ratio (PR) of the system. But on the other hand, the reduction of this capacity increases the theoretical power factor. This result shows that the SAPV system can cover the requested energy efficiently with a much lower battery capacity than in the case of the first scenario.

Table 4 Comparison of *PR* and *TPF* with reduced capacity of storage system

Performance Indicators	**Periods**			
	Low irradiance		High irradiance	
	Scenario I	Scenario II	Scenario I	Scenario II
PR	0.757	0.757	0.674	0.674
TPF	0.458	0.459	0.612	0.791

3.4 Influence of charge controller current capacity on the performance indicators

Simulation of scenario III is made to see the influence of charge controller current capacity on the performance indicators. Looking at the table 5, one can see that the PR is not influenced by the reduction of charge controller current capacity in either case of low or high irradiance. But in other hand, the reduction of charge controller current capacity influences crucially in decreasing the theoretical power factor of SAPV system. This last observation can be justified by the fact that current will be stopped at the charge controller even when the irradiance is high. This will cause a low charging of storage system and therefore increase the reactive energy made more by the uncharged (or unused) capacity storage.

Table 5 Comparison of *PR* and *TPF* with reduction of charge controller current capacity

Performance Indicators	Periods			
	Low irradiance		High irradiance	
	Scenario I	Scenario III	Scenario I	Scenario III
PR	0.757	0.757	0.674	0.674
TPF	0.458	0.458	0.612	0.458

3.5 Influence of inverter power capacity on the performance indicators

Simulation of scenario IV is made to see the influence of inverter power capacity on the performance indicators. Looking at table 6, one can see that, if in the precedent scenarios the PR is not influenced by the charge controller current capacity and capacity of storage system of SAPV system, in this last scenario the reduction of the inverter power capacity influence clearly the PR. It can be justified by the fact the if the inverter capacity is limited, all the energy demand will not be covered.

The reduction of inverter power capacity has also decreased TPF, this can be justified by the fact that the huge energy which can be stored in the battery is not sufficiently used at the end. Because of the low energy demand. The SAPV system should be size well regarding the scale of energy demand.

Table 6 Comparison of *PR* and *TPF* with reduction inverter Power capacity

Performance Indicators	Periods			
	Low irradiance		High irradiance	
	Scenario I	Scenario IV	Scenario I	Scenario IV
PR	0.757	0.757	0.674	0.674
TPF	0.458	0.458	0.612	0.600

4. CONCLUSION

The locations far from electricity distribution networks and those suffering from poor electricity quality often resort to stand-alone PV systems (SAPV) which now appear to be the best solution for access to electricity. the sizing methods for these systems are not perfect. It is therefore possible to install a system that is not very suitable for use. Indicators proposed by the IEA PVPS Task 2, when they are well calculated, make it possible to attenuate the errors related to the sizing. But these indicators do not always tell us about the capacity of the installed SAPV system actually used.

It is in this way that we have developed a new performance indicator called the theoretical power factor (TPF), by an original method based on the modelling of the SAPV system in the form of a matrix equation. this indicator informs us about the reactive energy of the SAPV system. The reactive energy is this energy which was solicited and installed but which is not used at the end.

In this work, we have described the system studied, presented the performance indicator most used in the literature, calculated from a case study the performance indicators (the new one and the one most used in the literature). We have also analysed the evolution of the reactive energy for the case study and observed the influence of the capacity of each main element of the SAPV system on the proposed performance indicator TPF and on the conventional performance indicator PR. The reduction of 40% of the main element capacity of the SAPV system (storage system, charge controller and inverter) in each different scenario, makes it possible to observe during the period of low irradiance, an increase in TPF of 0.1% in Scenario II and no change in TPF in Scenarios III and IV. During the period of high irradiance, an increase in TPF of 17.9% is observed in scenario II and a decrease in TPF of 15.4% and 1.2% respectively in scenarios III and IV.

which leads to the conclusion that a low capacity of the charge controller or the inverter is not conducive to the optimal use of the SAPV system, especially since these are the main points of conversion of electrical energy. However, an appropriate value for the storage capacity is very favourable to the optimal use of the SAPV system because it is one of the most sensitive points in the design and operation of SAPV systems

Acknowledgments

The authors are grateful to Patrice ELE ABIAMA, Head Manager of the National Committee for Development of Technologies (NCDT) for his valuable help and his supervision.

REFERENCES

[1] B. Pillot, M. Muselli, P. Poggi, et J. B. Dias, « Historical trends in global energy policy and renewable power system issues in Sub-Saharan Africa: The case of solar PV », *Energy Policy*, vol. 127, p. 113-124, 2019.

[2] T. Khatib, A. Mohamed, et K. Sopian, « A review of photovoltaic systems size optimization techniques », *Renew. Sustain. Energy Rev.*, vol. 22, p. 454-465, 2013.
[3] T. Khatib, I. A. Ibrahim, et A. Mohamed, « A review on sizing methodologies of photovoltaic array and storage battery in a standalone photovoltaic system », *Energy Convers. Manag.*, vol. 120, p. 430-448, 2016.
[4] T. Khatib, A. Mohamed, K. Sopian, et M. Mahmoud, « A New Approach for Optimal Sizing of Standalone Photovoltaic Systems », *Int. J. Photoenergy*, vol. 2012, p. e391213, févr. 2012, doi: 10.1155/2012/391213.
[5] J. Lian, Y. Zhang, C. Ma, Y. Yang, et E. Chaima, « A review on recent sizing methodologies of hybrid renewable energy systems », *Energy Convers. Manag.*, vol. 199, p. 112027, 2019.
[6] U. Jahn *et al.*, « International Energy Agency PVPS Task 2: Analysis of the operational performance of the IEA Database PV systems », in *Sixteenth European Photovoltaic Solar Energy Conference*, Routledge, 2020, p. 2673-2677.
[7] T. Nordmann, L. Clavadetscher, et U. Jahn, « PV system performance and cost analysis, a report by IEA PVPS Task 2 », in *Proceedings of the 22nd European Photovoltaics Solar Energy Conference, Milano*, 2007.
[8] A. Ameur, A. Berrada, K. Loudiyi, et M. Aggour, « Forecast modeling and performance assessment of solar PV systems », *J. Clean. Prod.*, vol. 267, p. 122167, 2020.
[9] R. Kumar, C. S. Rajoria, A. Sharma, et S. Suhag, « Design and simulation of standalone solar PV system using PVsyst Software: A case study », *Mater. Today Proc.*, vol. 46, p. 5322-5328, 2021.
[10] R. Srivastava, A. N. Tiwari, et V. K. Giri, « An overview on performance of PV plants commissioned at different places in the world », *Energy Sustain. Dev.*, vol. 54, p. 51-59, 2020.
[11] T. Ma, H. Yang, et L. Lu, « Long term performance analysis of a standalone photovoltaic system under real conditions », *Appl. Energy*, vol. 201, p. 320-331, 2017.
[12] H. M. Ridha, C. Gomes, H. Hizam, M. Ahmadipour, A. A. Heidari, et H. Chen, « Multi-objective optimization and multi-criteria decision-making methods for optimal design of standalone photovoltaic system: A comprehensive review », *Renew. Sustain. Energy Rev.*, vol. 135, p. 110202, 2021.
[13] P. Arun, R. Banerjee, et S. Bandyopadhyay, « Optimum sizing of photovoltaic battery systems incorporating uncertainty through design space approach », *Sol. Energy*, vol. 83, nº 7, p. 1013-1025, 2009.

Research Article

Energy, Environment and Storage (2023)03-02:52-58

Energy, Environment and Storage

Journal Homepage: www.enenstrg.com

Theoretical Study of The Use of Lfscs in Terms of Energy for Textile Factories: The Example of Saint Louis in Senegal

Issa SY[1*], İbrahim ÜÇGÜL[2]

[1]*Graduate School of Natural and Applied Sciences, Department of Renewable Energy, Süleyman Demirel University, Isparta, Turkey, ORCID: 0000-0001-9889-4783.*

[2]*Department of Textile Engineering, Faculty of Engineering, Süleyman Demirel University, Isparta, Turkey, 0000-0001-9794-0653.*

ABSTRACT. Senegal has a high potential for solar energy but mainly depends on fossil energy resources. Industries, particularly the textile sector, could benefit from the use of alternative energy sources to reduce costs and improve the environmental footprint. This study focuses on the use of linear Fresnel solar collectors (LFSC) coupled with an Organic Rankine Cycle (ORC) system to produce energy in textile mills, particularly in Saint Louis. The objective was to size a Fresnel solar array and evaluate its energy production for two different periods: the sunniest month (April) and the least sunny month (August). The findings demonstrate the substantial solar potential of the region, with significant sunshine throughout the year. The maximum direct solar radiation recorded on August 15 and April 25 was 898 W/m2 and 945 W/m2, respectively, at noon. The maximum energy production for one row in August is 24.4 kWh, and in April, it reaches 25.7 kWh. It is noted that, for the use of the Fresnel linear system, the number of rows will depend on the energy needs of the textile factory.

Keywords: *Solar energy, Linear Fresnel Reflector, concentrating solar power, Senegal.*

Article History: Received: 15.03.2023; Accepted:19.03.2023; Available Online: 29.05.2023
Doi: https://doi.org/10.52924/PIBX6890

1. INTRODUCTION

Located in the extreme west of Africa between 12°5 and 16°5 North latitude and 11°5 and 17°5 West longitude, Senegal covers an area of 196.712 km2. Like many countries in Africa, solar energy is abundant in Senegal. The whole country is sunny and receives a level of global horizontal sunshine between 2045 and 2191 kWh/m2 /year and 1461 of 1607 kWh/m2 /year of direct radiation. That is 3,000 hours of sunshine per year and an average daily solar irradiation of 5.8 kWh/m2/day [1]. The solar potential maps show that the global horizontal irradiation (GHI) in the centre and north averages about 2170 kWh/m²/year. For direct normal irradiation (DNI), the annual average is about 1607 in a large part of the north, like Saint Louis. The energy sector is essentially dependent on the outside world due to the predominance of fossil energy resources (petroleum products and other hydrocarbons) which the country does not possess. Although the country has many natural resources whose energy potential is proven very little exploited.

Senegal's exports have grown stronger thanks to the development of manufacturing industries. After independence, industries diversified and improved the quality of their products to meet the growing demand of the domestic market and neighbouring countries. In the textile sector, the use of solar energy can be a promising solution to reduce operating costs and improve the environmental footprint of the industry.

Production costs have increased considerably with the rise in energy prices, and this can affect the competitiveness of companies. Thus, the use of alternative energy sources is becoming an important option for these industries [2]. In this respect and with the current context of climate change, there is a need to think about the use of more sustainable resources[3]. Renewable energy resources are seen as one of the most efficient solutions [4]. Alrikabi et al (2014) [5] worked on the types of renewable energy sources. Their results show that by promoting renewable energy, air pollution, soil pollution and water pollution can be avoided and a country's economy will increase. The use of renewable energies and particularly solar thermal energy is one of the most promising strategies [6]. The production of thermal energy is based on concentrating solar power technologies. These technologies use collectors to concentrate solar radiation onto absorbers, which heat a heat transfer fluid to a high temperature. This fluid can then be used to generate electricity [7]. Two

types of solar concentrators can be distinguished: point concentrators, which track the sun on two axes, such as tower plants and Stirling Dish plants, and linear concentrators, which track the sun on one axis, such as parabolic trough concentrators and Fresnel mirrors [8]. These systems offer several advantages, such as their ability to concentrate sunlight and their suitability for industrial applications [9]. Industries, known for their substantial energy consumption, can particularly benefit from the integration of LFSCs to reduce their reliance on fossil fuels [10].

This study focuses on investigating the potential of LFSCs for energy production in textile factories, using the case of Saint Louis in Senegal as an example. By examining the technical aspects of LFSC implementation in this specific context, this study aims to provide valuable insights for similar settings globally. The primary objective of this research is to assess the energy output of LFSCs in textile factories, employing an Organic Rankine Cycle (ORC) system as a conversion mechanism. By analyzing the results at different times of the year, this study aims to determine the system's performance under varying solar conditions. To achieve these objectives, a theoretical approach is adopted, encompassing the sizing of the Fresnel solar array and the evaluation of energy production.

Overall, this theoretical study serves as a foundation for assessing the feasibility and potential benefits of integrating LFSCs in textile factories, taking into account the specific case of Saint Louis in Senegal. The findings will not only contribute to the existing knowledge on solar energy utilization but also provide valuable insights for industries seeking sustainable energy solutions. This work will be one of the first steps in the use of Linear Fresnel Solar Collectors in the area.

2. SOLAR ENERGY

2.1 Solar radiation

Solar energy is an energy source that comes from the sun's rays. It is considered to be the most powerful source of energy and is also free and easy to use. The calculation of the total incident solar radiation on an exposed surface depends on several factors, such as the geographical position of the surface, the time of day, the season, the orientation and inclination of the surface, and the weather conditions. Direct radiation is given by:

$$I_d = I_{DN} \times \cos(\theta_s) \quad (1)$$

With θ_s the value of the angle of incidence of the sun.
And

$$I_{DN} = A_1 \times \exp\left(-\frac{P_L}{P_o} \times \frac{B}{\sin(h)}\right) \quad (2)$$

Where:

$\frac{P_L}{P_o}$ is the pressure ratio at the location concerned with the standard atmospheric pressure.

A_1 is the extraterrestrial solar intensity.

B is the atmospheric absorption coefficient.

h is the angular height

$$\frac{P_L}{P_o} = \exp(-0.0001184 \times H_{alt}) \quad (3)$$

$$A_1 = 1158 \times \left[1 + 0.066 \times \cos\left(360 \times \frac{n}{370}\right)\right] \quad (4)$$

$$B = 0.175 \times [1 - 0.2 \times \cos(0.93 \times n)] - 0.0045 \times [-\cos(1.86 \times n)] \quad (5)$$

H_{alt} is the altitude in metres above sea level.

n is the number of days in the year between 1 and 365 or 366 (leap year).

2.2 Solar energy technologies

Technologies for the exploitation of solar energy are divided into two categories: active and passive technologies. Active technologies convert solar energy directly into electrical or thermal energy, such as photovoltaic cells, solar collectors, solar concentrators, solar heating and cooling systems, and solar cookers. Passive technologies, on the other hand, focus on the orientation of buildings to the sun and the use of special materials and architectural designs to harness solar energy [11].

Solar concentrators usually consist of two components: the concentrator and the receiver. The concentrator reflects the sun's rays to the receiver. The receiver acts as a heat exchanger that converts the solar flux reflected by the mirrors into heat. This heat is then used to produce electrical energy or for cogeneration. There are four main technologies of concentrating solar power plants for electricity generation: the tower plant, the parabolic trough plant, the parabolic or Dish plant and the linear Fresnel plant [12].

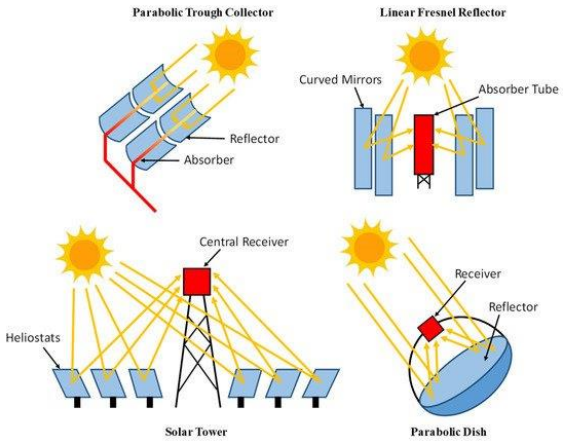

Fig. 1. Different types of solar concentrators [13]

Fresnel technology uses flat mirrors arranged to form a parabolic cylinder shape. These mirrors are equipped with a motorised system that allows them to follow the sun on a single axis, to concentrate the rays towards a linear receiver located on the focal length. This solar power plant uses a working fluid, which can be oil or water [14].

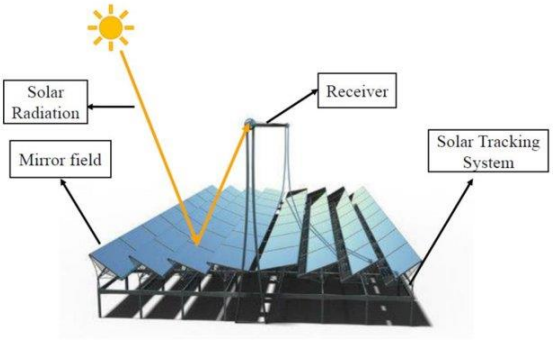

Fig. 2. Linear Fresnel Reflector system representation *[15]*

Linear Fresnel collectors have been used because they have the advantage of being cheaper to produce and install. They also require less reflective material and are easier to maintain. In addition, linear Fresnel collectors can be more flexible in terms of size and shape, which can be an advantage for projects where space is limited. They can also be adapted to operate with different working fluids, such as oil or water, allowing them to meet a variety of energy needs.

3. METHODOLOGY

3.1 Model sizing

The Fresnel concentrator principle is based on mirrors that can be rotated to follow the path of the sun to permanently redirect and concentrate the sun's rays to a fixed linear receiver tube or set of tubes. By circulating through this horizontal receiver, a thermodynamic liquid of up to 550°C can be vaporised and superheated. The steam produced then drives a turbine which generates electricity [16].

According to [17] linear Fresnel solar collectors can be designed using two different methods. In the first method, a fixed receiver width and height are chosen, from which variable mirror dimensions, mirror angles and inter-mirror distances can be calculated. In the second method, the one used in this work, the mirror widths and receiver height are fixed and the other device parameters are determined by simple equations.

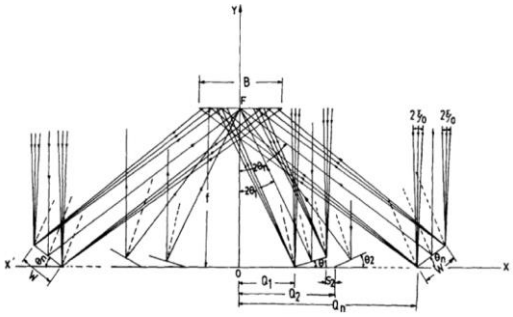

Fig. 3. Schematic modelling of an LFRSC *[17]*

In this model, each mirror is characterised by three parameters:

- ✓ the angle of the mirrors θ_n ;
- ✓ the distance between the mirror and the receiver Q_n ;
- ✓ the offset between two adjacent mirrors S_n.

$$\theta_n = \frac{1}{2}\tan^{-1}\left[\frac{Q_n+\frac{W}{2}\cos(\theta_{n-1})}{f+\frac{W}{2}\sin(\theta_{n-1})}\right] \quad (6)$$

$$Q_n = Q_{n-1} + W \times \cos(\theta_{n-1}) + S_n \quad (7)$$

$$S_n = W \times \sin(\theta_{n-1}) \times \tan(2\theta_n + \xi_0) \quad (8)$$

In these equations:

W is the width of the mirrors, f the height of the absorber above the plane mirrors and the index n is the mirror number.

ξ_0 is half the apparent angle of the sun at any point on the Earth. The initial values of the various design parameters are given [17] :

$$\theta_0 = 0, \xi_0 = 16° , S_1 = 0 , Q_1 = \frac{W}{2} \text{ et } Q_0 = -\frac{W}{2} .$$

The receiver width design can be calculated based on the data calculated for the last mirror using the formula below.

$$B = 2\left[\left(Q_k + \frac{W}{2}\cos\theta_k\sec 2\theta_k\right)\frac{\sin\xi_0}{\sin 2\theta_k\cos(2\theta_k+\xi_0)} + \frac{W}{2}\cos\theta_k\sec 2\theta_k\right] \quad (9)$$

Here k represents the number of mirrors in a dimension.

The concentration ratio (CR) of the Fresnel collector can be determined by adding the concentration contribution of the mirrors (CIn).

$$CR = 2\sum_{n=1}^{n=k} CI_n \quad (10)$$

$$CIn = \frac{W\times\cos\theta_n}{U_n+D_n+I_n} \quad (11)$$

With U_n, D_n and the values of the reflected solar rays.

$$U_n = \left(\frac{Q_n+W\cos\theta_n-\frac{W}{2}\cos\theta_n\sec 2\theta_n}{\sin 2\theta_n}\right)\frac{\sin\xi_0}{\cos(2\theta_n-\xi_0)} \quad (12)$$

$$D_n = W \times \cos\theta_n\sec 2\theta_n \quad (13)$$

$$I_n = \left(\frac{Q_n+\frac{W}{2}\cos\theta_n\sec 2\theta_n}{\sin 2\theta_n}\right)\frac{\sin\xi_0}{\cos(2\theta_n-\xi_0)} \quad (14)$$

3.2 Energy balance and efficiency

The useful thermal power of the solar array is calculated by subtracting the thermal losses from the total absorbed power [18].

$$Q_{field} = Q_{inc} - Q_{loss} \quad (15)$$

The thermal power absorbed by the absorber tube and the thermal losses of the Fresnel field are calculated according to [18].

$$Q_{inc} = \eta_{opt,0} \times K_t \times K_l \times \eta_{endloss} \times cl \times \chi_{field} \times A_{ST} \times I_d \quad (16)$$

$$Q_{loss} = A_{field} \times 0.0724\frac{W}{m^2} \times (-0.389 \times \Delta T + 0.0108 \times \Delta T^2) + A_{ST} \times q_{pipeloss} \quad (17)$$

In these equations, $\eta_{opt,0}$ is the efficiency of the optical collector for the perpendicular sun on collector, cl being the average cleaning factor, χ_{field} being the solar field availability, A_{ST} is the total collector opening area and ΔT is the temperature difference between the average

temperature of the fluid in the solar field and the ambient temperature.

$$\Delta T = \frac{T_{in}+T_{out}}{2} - T_{amb} \quad (18)$$

$\eta_{endloss}$ is the final loss efficiency, it describes the amount of the receiver that is not illuminated by the reflected rays [19].

$$\eta_{endloss} = 1 - \frac{f \times \tan(\theta_l)}{Lm} \quad (19)$$

$K_t(\theta_t)$ is the correction factor for the angle of incidence in the transverse plane;

$K_l(\theta_l)$ is the correction factor for the angle of incidence in the longitudinal plane[20].

$$K_l(\theta_l) = \cos(\theta_l) - \frac{f}{L_m}\sqrt{1+\left(\frac{W_D}{4f}\right)^2} \times \sin(\theta_l) \quad (20)$$

$$K_t(\theta_t) = \begin{cases} \cos\left(\frac{\theta_t}{2}\right) - \frac{\frac{W_D}{4}}{f+\sqrt{f^2+\left(\frac{W_D}{4f}\right)^2}} \times \sin\left(\frac{\theta_t}{2}\right), & \text{when the } \theta_t < \theta_{t,crit} \\ \cos\left(\frac{\theta_t}{2}\right) - \frac{\frac{W_D}{4}}{f+\sqrt{f^2+\left(\frac{W_D}{4f}\right)^2}} \times \sin\left(\frac{\theta_t}{2}\right) \times \left[\frac{D_W}{W} \times \frac{\cos(\theta_t)}{\cos\left(\frac{\theta_t+\varphi_m}{2}\right)}\right], & \text{when the } \theta_t \geq \theta_{t,crit} \end{cases} \quad (21)$$

Where:

$$\varphi_m = 2\arctan \frac{\frac{W_D}{4}}{\left[f+\sqrt{f^2+\left(\frac{W_D}{4f}\right)^2}\right]} \quad (22)$$

And:

$$\theta_{t,crit} = 94.46 - 2.519\frac{W}{D_W} - 55.71\left(\frac{W}{D_W}\right)^2 - 0.48\varphi_m + 1.77\frac{{\varphi_m}^2}{1000} + 1.15\frac{W}{D_W}\varphi_m \quad (23)$$

Equations (19) and (20) are valid only for 20°< φ_m <70° and 0.50 < ($\frac{W}{D_W}$) <0.95 [21].

4. RESULTS AND DISCUSSIONS

4.1 The parameters of the Fresnel system model

The MATLAB program was used to calculate the mirrors and their distances and the results are given in Table 1. In the calculations, the width of the mirrors W was fixed at 0.40 m, the length at 40 m and the height of the absorber above the plane mirrors f to 6 m.

Table 1 Result of the mirror data of the linear Fresnel collector.

	M 1	M 2	M3	M 4	M 5	M 6	M7
Q	0.20	0.60161	1.00618	1.41555	1.82998	2.25131	2.68086
θ	1.907	3.8002	6.1181	7.5044	9.3011	11.0468	12.7385

It is important to note that these results were obtained for one side of the receiver. Being symmetrical, the same data is used for the other side. After calculating all the necessary parameters for the mirror, the width of the receiver found according to the data calculated for the last mirror is 0.502 m.

The concentration ratio (CR) of the Fresnel collector can be determined by adding the concentration contribution of the mirrors (CIn). The results are given in Table 2.

Table 2 Result of Condensation Rate Coefficients and Condensation Rate vs. Mirrors.

	A	Dn	In	Cln
Mirror 1	2.8003	40.0666	2.8065	0.8753
Mirror 2	2.8362	40.2658	2.8488	0.8686
Mirror 3	2 .6947	40.6967	2.7154	0.8626
Mirror 4	2.9861	41.0580	3.0121	0.8428
Mirror 5	3.0994	41.6501	3.1329	0.8244
Mirror 6	3.2419	42.3700	3.2833	0.8029
Mirror 7	3.4142	43.2181	3.4645	0.7788
Total on one side				**5.8554**
Concentration ratio				**11.71075**

4.2 Solar Irradiation and thermal energy

According to the meteorology of the site, the energy production was calculated in August with the lowest direct solar radiation and in April with good radiation [22]. The amount of direct solar radiation (Id) and the instantaneous thermal energy (Qfield) that can be provided by the solar field was obtained from 07:00 to 17:00 on August 15 and April 25.

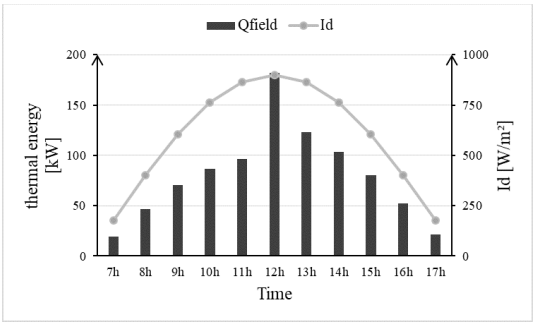

(a) August

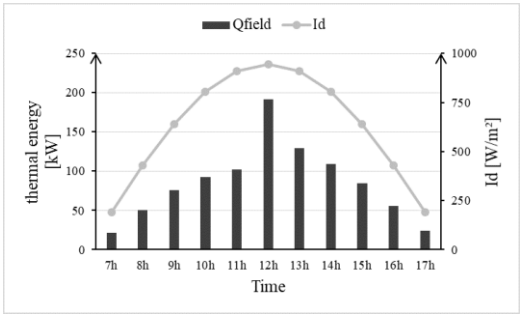

(b) April

Fig. 4. Direct solar radiation and instantaneous thermal energy on August 15 (a) and April 25 (b).

Fig. 4 shows the amount of direct solar radiation and the instantaneous thermal energy that the solar field can provide, measured from 7:00 am to 5:00 pm on August 15

(a) and April 25 (b). The results show that the region has a large solar potential and that all months have significant sunshine.

4.3 Energy production with the organic Rankine cycle (ORC)

The organic Rankine cycle is a thermodynamic process used to convert heat into electrical energy using the system's output temperature. The choice of organic fluid used in the ORC system is critical for its efficiency and performance. For this process, R152a was chosen as the organic fluid. According to [23], it gives a good working efficiency of the turbine and a high cycle efficiency. The energy production calculations were carried out using the Solkane 8 software. The input parameters are as follows: T_{Evap} = 100 °C, T_{cond} = 40 °C, Turbine-efficiency = 0.98 and Pump- efficiency = 0.89. To evaluate the electrical energy produced by the ORC turbine system, the amounts of useful heat transferred to the heat transfer fluid between 7 a.m. and m. were taken in Table 3. These data were collected for one row on August 15 and April 25.

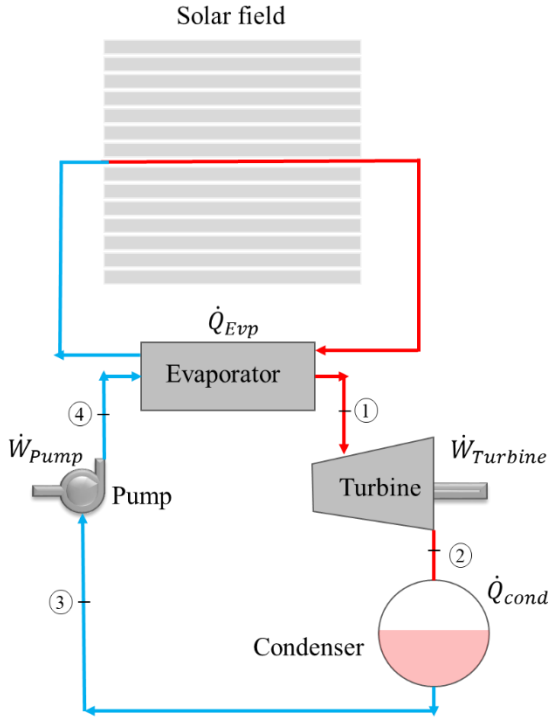

Fig. 5. ORC system representation.

Table 3 The values of energy production obtained by a row of the organic Rankine system.

Time	$\dot{Q}_{Evp}$ (kWh)	$\dot{Q}_{cond}$ (kWh)	$\dot{W}_{Turbine}$ (kWh	$\dot{W}_{Pump}$ (kWh)	$\dot{W}_{net}$ (kWh)	η_{th}
7h	19.45	17.04	2.66	0.28	2.6	0.12
8h	46.87	41.07	6.4	0.68	6.28	0.12
9h	70.62	61.89	9.65	1.03	9.46	0.12
10h	86.66	75.9	11.8	1.3	11.6	0.12
11h	96.56	84.6	13.2	1.4	12.9	0.12
12h	181.87	159.4	24.9	2.6	24.4	0.12
13h	123.13	107.9	16.8	1.8	16.5	0.12
14h	103.39	90.6	14.1	1.5	13.8	0.12
15h	79.96	70.1	10.9	1.2	10.7	0.12
16h	51.97	45.54	7.1	0.76	6.96	0.12
17h	21.47	18.81	2.93	0.31	2.88	0.12

(a) August

Time	$\dot{Q}_{Evp}$ (kWh)	$\dot{Q}_{cond}$ (kWh)	$\dot{W}_{Turbine}$ (kWh)	$\dot{W}_{Pump}$ (kWh)	$\dot{W}_{net}$ (kWh)	η_{th}
7h	21.61	18.94	2.95	0.31	2.89	0.12
8h	50.51	44.26	6.9	0.74	6.76	0.12
9h	75.47	66.1	10.3	1.1	10.1	0.12
10h	92.30	80.9	12.6	1.3	12.4	0.12
11h	101.87	89.3	13.9	1.5	13.6	0.12
12h	191.56	167.9	26.2	2.8	25.7	0.12
13h	129.15	113.2	17.6	1.9	17.3	0.12
14h	108.83	95.4	14.9	1.6	14.6	0.12
15h	84.74	74.3	11.6	1.2	11.3	0.12
16h	55.59	48.71	7.6	0.81	7.44	0.12
17h	23.69	20.76	3.24	0.35	3.17	0.12

(b) April

The table above shows the values of energy production obtained by a row of the organic Rankine system on 15 August (a) and 25 April (b). In this context, the expressions $\dot{Q}_{Evp}$ represent the amount of energy entering the evaporator (kWh), $\dot{Q}_{cond}$ the amount of energy drawn from the condenser (kWh), $\dot{W}_{Turbine}$ the amount of energy obtained in the turbine (kWh), $\dot{W}_{Pump}$ the amount of energy needed to operate the pump (kWh), and finally $\dot{W}_{net}$ corresponds to the net electricity produced by the system (kWh). The cycle efficiency is defined as the ratio between the net powers of the cycle to the evaporator heat rate. The results show that the maximum amount of energy obtained in August is 24.4 kWh, while in April it reaches 25.7 kWh. Despite a slightly small difference, both values indicate a high solar potential in the region. Indeed, all months of the year are almost equally sunny, with a slight variation. These results have implications for the size of a linear Fresnel system, which will depend on

the energy needs of the textile factory. For example, to produce 500 kWh, 20 collector rows would be required.

5. CONCLUSION

The use of linear Fresnel solar collectors in textile mills can have many economic and environmental benefits. This work focused on the use of linear Fresnel solar collectors (LFSC) for energy production in textile factories, using the example of Saint Louis, Senegal. After sizing the Fresnel solar array, the energy output was assessed using the ORC at two distinct times: the month with the most sunshine (April) and the month with the least sunshine (August). The organic fluid R152a and the Solkane program were used to calculate the electricity production.

The results show that the region has a large solar potential and that all months have significant sunshine. According to the calculations, the maximum direct solar radiation obtained on August 15 and April 25 was 898 W/m^2 and 945 W/m^2, respectively. These values were produced at 12:00 pm. With a single collector row, energy production amounts to 24.4 kWh during the month of August, while in April it reaches 25.7 kWh. In addition, the thermal efficiency of the system is 12%. To optimise the needs of a textile factory it is necessary to multiply the number of rows. The use of this technology is a viable solution for companies seeking to reduce their dependence on fossil fuels and improve their environmental impact. Therefore, it is important that companies study the economic cost of implementing such a system of linear Fresnel solar collectors for energy production.

REFERENCES

[1] N. Diaw and T. T. Soe, 'Estimation of Solar Potential in Senegal Using GIS Application', *International Journal of Advanced Research*, vol. 4, no. 1, p. 5, 2017.

[2] B. Tchanche, 'Analyse du système énergétique du Sénégal', *Revue des Energies Renouvelables*, vol. 21, no. 1, pp. 73–88, 2018.

[3] Y. Mochizuki and A. Bryan, 'Climate Change Education in the Context of Education for Sustainable Development: Rationale and Principles', *Journal of Education for Sustainable Development*, vol. 9, no. 1, pp. 4–26, Mar. 2015, doi: 10.1177/0973408215569109.

[4] I. Dincer, 'Renewable energy and sustainable development: a crucial review', *Renewable and Sustainable Energy Reviews*, vol. 4, no. 2, pp. 157–175, Jun. 2000, doi: 10.1016/S1364-0321(99)00011-8.

[5] N. Kh. M. A. Alrikabi, 'Renewable Energy Types', *JOCET*, vol. 2, no. 1, pp. 61–64, 2014, doi: 10.7763/JOCET.2014.V2.92.

[6] D. Qerimi, C. Dimitrieska, S. Vasilevska, and A. A. Rrecaj, 'Modeling of the Solar Thermal Energy Use in Urban Areas', *Civ Eng J*, vol. 6, no. 7, pp. 1349–1367, Jul. 2020, doi: 10.28991/cej-2020-03091553.

[7] V. Siva Reddy, S. C. Kaushik, K. R. Ranjan, and S. K. Tyagi, 'State-of-the-art of solar thermal power plants—A review', *Renewable and Sustainable Energy Reviews*, vol. 27, pp. 258–273, Nov. 2013, doi: 10.1016/j.rser.2013.06.037.

[8] M. Saini, A. Sharma, V. P. Singh, G. Dwivedi, and S. Jain, 'Solar Thermal Receivers—A Review', in *Advancement in Materials, Manufacturing and Energy Engineering, Vol. II*, P. Verma, O. D. Samuel, T. N. Verma, and G. Dwivedi, Eds., in Lecture Notes in Mechanical Engineering. Singapore: Springer Nature, 2022, pp. 311–325. doi: 10.1007/978-981-16-8341-1_25.

[9] K. B. Kumar, M. Gupta, and D. S. Mehta, 'Efficient sunlight harvesting with combined system of large Fresnel lens segmented mirror reflectors and compound parabolic concentrator without tracking sun for indoor daylight illumination', *Renewable Energy*, vol. 202, pp. 1198–1214, Jan. 2023, doi: 10.1016/j.renene.2022.11.117.

[10] F. J. Sepúlveda *et al.*, 'Analysis of Potential Use of Linear Fresnel Collector for Direct Steam Generation in Industries of the Southwest of Europe', *Energies*, vol. 12, no. 21, p. 4049, Oct. 2019, doi: 10.3390/en12214049.

[11] C. Firat and K. Çalik, 'Electrical and Thermal Performance Analysis of a Linear Fresnel Reflector-Photovoltaic/Thermal System', *Academic Platform Journal of Engineering and Science*, vol. 9, no. 2, pp. 264–273, May 2021, doi: 10.21541/apjes.778563.

[12] A.-G. Jolivot, 'Conception et dimensionnement d'un récepteur linéaire pour un concentrateur de type Fresnel', 2015.

[13] M. Toub, C. R. Reddy, R. D. Robinett, and M. Shahbakhti, 'Integration and Optimal Control of MicroCSP with Building HVAC Systems: Review and Future Directions', *Energies*, vol. 14, no. 3, p. 730, Jan. 2021, doi: 10.3390/en14030730.

[14] M. J. Montes, C. Rubbia, R. Abbas, and J. M. Martínez-Val, 'A comparative analysis of configurations of linear Fresnel collectors for concentrating solar power', *Energy*, vol. 73, pp. 192–203, Aug. 2014, doi: 10.1016/j.energy.2014.06.010.

[15] P. Scalco, J. Copetti, M. H. Macagnan, and J. Diehl de Oliveira, 'Linear Fresnel Solar Collector Concentrator - A Review', in *Proceedings of the 26th International Congress of Mechanical Engineering*, ABCM, 2021. doi: 10.26678/ABCM.COBEM2021.COB2021-0132.

[16] M. Ghodbane, B. Boumeddane, Z. Said, and E. Bellos, 'A numerical simulation of a linear Fresnel solar reflector directed to produce steam for the power plant', *Journal of Cleaner Production*, vol. 231, pp. 494–508, Sep. 2019, doi: 10.1016/j.jclepro.2019.05.201.

[17] S. S. Mathur, T. C. Kandpal, and B. S. Negi, 'Optical design and concentration characteristics of linear Fresnel reflector solar concentrators—II. Mirror elements of equal width', *Energy Conversion and Management*, vol. 31, no. 3, pp. 221–232, Jan. 1991, doi: 10.1016/0196-8904(91)90076-U.

[18] G. Morin, J. Dersch, W. Platzer, M. Eck, and A. Häberle, 'Comparison of Linear Fresnel and Parabolic Trough Collector power plants', *Solar Energy*, vol. 86, no. 1, pp. 1–12, Jan. 2012, doi: 10.1016/j.solener.2011.06.020.

[19] Y. Elmaanaoui and D. Saifaoui, 'Parametric analysis of end loss efficiency in linear Fresnel reflector', in *2014 International Renewable and Sustainable Energy Conference (IRSEC)*, Ouarzazate, Morocco: IEEE, Oct. 2014, pp. 104–107. doi: 10.1109/IRSEC.2014.7059813.

[20] E. Bellos, 'Progress in the design and the applications of linear Fresnel reflectors – A critical review', *Thermal Science and Engineering Progress*, vol.

10, pp. 112–137, May 2019, doi: 10.1016/j.tsep.2019.01.014.
[21] M. Ghodbane, Z. Said, A. A. Hachicha, and B. Boumeddane, 'Performance assessment of linear Fresnel solar reflector using MWCNTs/DW nanofluids', *Renewable Energy*, vol. 151, pp. 43–56, May 2020, doi: 10.1016/j.renene.2019.10.137.
[22] 'Saint-Louis : Climat, Températures et Météo. Les meilleures périodes !(SENEGAL)', *www.partir.com*. https://www.partir.com/Senegal/Saint-Louis/2246452/quand-partir.html (accessed Mar. 13, 2023).
[23] P. Prabowo., A. G.T., and E. Ekadewi., 'Performance of Organic Rankine Cycle in Different Refrigerants for Low Temperature Geothermal using Delphi Program', *jtm*, vol. 12, no. 2, pp. 102–108, Jun. 2011, doi: 10.9744/jtm.12.2.102-108.

Energy, Environment and Storage

Journal Homepage: www.enenstrg.com

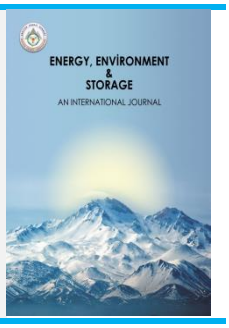

Optimization of the Effects of Binary Hybrid Nanofluid Synthesis Parameters on the Thermal and Hydraulic Characteristics

Orhan Keklikcioglu[1*], Veysel Ozceyhan [2]

[1]*Erciyes University,Department of Mechanical Engineering,ORCID: 0000-0002-6227-3130*
[2]*Erciyes University,Department of Mechanical Engineering, ORCID: 0000-0003-3829-9477*

ABSTRACT. Due to the growing interest in hybrid nanofluids, researchers have been primarily focused to obtain the thermophysical properties of hybrid nanofluids. Several parameters such as temperature, volume or weight fractions, nanoparticle types and shapes affected the thermophysical properties of nanofluids. Accordingly, the optimization in thermal conductivity and viscosity of nanofluids obtained by mixing binary nanocomposite particles GnP-Fe_3O_4 in an ethylene glycol-water base fluid with a mixing ratio of 20-80 % was investigated in this study. The Taguchi approach is used for single-objective optimization and the significance values of the synthesis parameters were determined using the ANOVA technique. Five different factors, including mechanical strring time, ultrasonic mixing time and power, surfactant mixing ratio, and nanofluid weight ratio, were optimized at three different levels during the synthesis of hybrid nanofluids. The experimental $L_{27}(3^5)$ orthogonal array trial was built in order to carry out the optimization. According to the results, mechanical striring time was found to have the least impact on both thermophysical parameters, whereas ultrasonic mixing power, nanofluid weight ratio, and ultrasonic mixing time were also ranked from low to high impact. The usage of surfactant was shown to be the parameter that had the greatest impact, with rates of 63.57% and 65.31%, on thermal conductivity and viscosity, respectively.

Keywords: Taguchi ANOVA, Nanofluid, Thermal conductivity, Viscosity

Article History: Received: 31.03.2023; Accepted: 09.04.2023; Available Online: 29.05.2023
Doi: https://doi.org/10.52924/YWFM2644

1. INTRODUCTION

Heat control in thermal systems is considered one of the most common problems of today, and numerious studies are being conducted on the removal, recovery and storage of the energy from the thermal system [1-4]. Nanofluids have demonstrated their ability to be used in applications such as energy storage, heat exchangers, and heat sinks, resulting in improved heat transfer performance. The determination of the thermophysical properties of nanofluids that increase heat transfer rate in thermal systems has also become a precondition in order to reveal the activity mechanisms of nanofluids. Studying the thermophysical characteristics of hybrid nanofluids is mostly done to identify methods for enhancing cooling systems. [5]. The temperature of the nanofluid, particle fraction, base fluid type, nanoparticle size, shape, and type all affect the thermophysical properties of the nanofluid, such as specific heat, viscosity, and thermal conductivity [6]. Therefore, the evaluation of thermal conductivity focuses on improving heat transfer, while viscosity is evaluated for its effect on pressure drop under the same flow conditions.

Nowadays, nanotechnology enables the development of new types of nanofluid called composite or hybrid, which are obtained by mixing two or more nanoparticles with the base fluid. Despite ongoing research on nanofluids, it is evident that the studies focusing on the application of hybrid nanofluids in heat transfer are both contemporary and insufficient [7,8].

The thermal conductivity of a ZnO/TiO_2/EG hybrid nanofluid was studied by Toghraiel et al. [9] in the temperature range of 25 to 50°C and in the particle volume fraction range of 0 to 3.5%. The highest temperature and volume fraction were identified as generating hybrid nanofluids with the maximum thermal conductivity. The thermal conductivity of Al_2O_3-Cu/water hybrid nanofluids with volume concentrations ranging from 0.1% to 2% was examined by Suresh et al. [10]. For a volume concentration of 2%, the experimental measurement of thermal conductivity revealed a maximum improvement of 12.11%. Experimental research on the viscosity of TiO_2-Ag/engine oil and Al_2O_3-Ag/engine oil nanofluids was conducted by Liu et al. [11]. They claimed that as particle loading increases, viscosity decreases. Hemmat Esfe et al. [12]

*Corresponding author: keklikcioglu@erciyes.edu.tr

investigated at the Cu/TiO_2-water/EG hybrid nanofluid's thermal conductivity. At various composition concentrations (0.1, 0.2, 0.4, 0.8, 1, 1.5, and 2%) and temperatures ranging from 30 to 60 °C, the thermal characteristics of this nanofluid were measured. According to the findings, hybrid nanofluids' thermal conductivity improved as particle loading and temperature increased. The effects of temperature and particle concentration on the dynamic viscosity of the MgO-MWCNTs/EG hybrid nanofluid were investigated by Soltani and Akbari [13]. It was found that the dynamic viscosity can rise by up to 168% as the solid volume fraction rises from 0.1 to 1%.

As mentioned earlier, several factors, including the ratio of nanofluid to nanoparticle concentration, the type of nanoparticle, whether it is used in mono or hybrid applications, and the synthesis method, affect the thermal and hydraulic properties of nanofluids. In this case, the effects of these various characteristics have been investigated through optimization studies. By experimenting with several nanoparticles, including graphite, alumina, and zirconia, Abdullah et al. [14] were able to identify the best nano-oil combination. Using the Taguchi L_9 orthogonal array, the impact of parameters that included various quantities of surfactants and sonication time was examined. In comparison to the other samples, it was determined that the zirconia nanoparticle with SDBS surfactant and 10 minutes of sonication were the most ideal parameters for determining the stability of nano-oil. According to Rubasingh and Selvakumar [15], Taguchi design and Grey relational analysis were the most alluring approaches for taking into account the impact of the volume fractions (1 vol.%, 2 vol.%, 4 vol.%, and 8 vol.%) of TiO_2/ZnO nanocomposite on impressive thermophysical properties for the thermal performance of nanofluids. The stability of Al_2O_3/water nanofluids was investigated by Choudhary et al. [16] utilizing zeta potential analysis. The parameter that can interfere with the stability and thermal conductivity of nanofluids is optimized using the Taguchi method. S. Ravi Babu and G. Sambasiva Rao [17] employed the Taguchi technique to examine the stability of aqueous aluminum oxide, and the nanoparticle volume concentration, surfactant volume concentration, and sonication time were the variables used for optimization. They claimed that the stability of the nanofluid is closely correlated with the volume fraction, sonication time, pH level, and the ratio of surfactant volume to nanoparticle volume. The orthogonal layer (L_{25}) of the Taguchi design experiment was organized.

The authors noted that the thermal and hydraulic properties of base fluids are impacted by the unary or binary use of nanoparticles. The authors also discovered that factors like nanofluid fraction and synthesis methods improve the general properties of nanofluids. Thus, in this paper, the Taguchi method is used to assess the effects of mechanical stirring, ultrasonic sonication time and power, surfactant mixing ratios, and volume fractions with multi-levels on the thermal conductivity and viscosity of a binary hybrid GnP-Fe_30_4/water-ethylene glycol nanofluid. ANOVA, in addition to the Taguchi approach, is a contributing methodology for determining statistically significant variance between the means of independent parameters. The ANOVA and Taguchi techniques are utilized combined in the current study due to the significance of the data they provide, and no previous research has presented such an approach to the thermal conductivity and viscosity of the binary hybrid nanofluid of synthesis techniques. In this regard, it is a significant study in terms of applying a comparable approach to the hybrid nanofluids and getting qualified results with a little number of measurements.

2. MATERIALS AND METHODS

2.1 Synthesis of nanofluids

In this study, the synthesis approach of GnP/Fe3O4 water-ethylene glycol nanofluid is optimized to determine the influence of the technique on thermal conductivity and viscosity. The method used varies with 0.5, 0.75, and 1% weight fractions, surfactant/nanoparticle fractions of 1/10, 2/10, and 3/10, mechanical stirring times of 10, 20, and 30 minutes, ultrasonic sonication times of 30, 45, and 60 minutes, and sonification powers of 80, 100, and 120 watts.

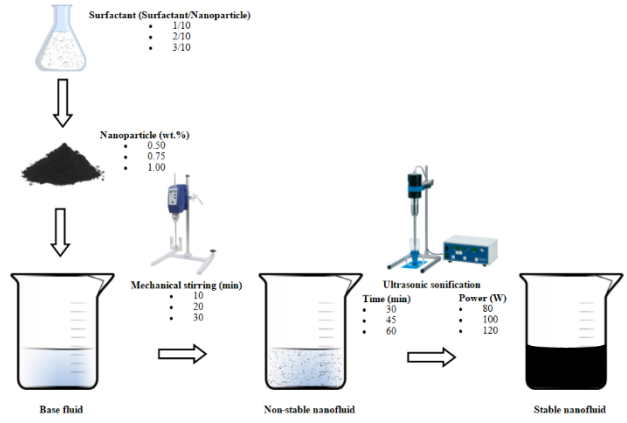

Fig. 1. Schematics of used technique to prepare nanofluid

Fig. 2. Nanofluid preparation and property measurement setup

Table 1 The thermophysical properties of nanoparticles [18].

Properties	GnP	FE_3O_4
Specific heat (J/kgK)	790	104
Density (kg/m3)	2250	5180
Thermal conductivity (W/mK)	3000	17.65
Particle size(nm)	3	12-29
Purity	>99.9%	>99.5%

GnP and Fe_3O_4 nanoparticles, whose thermophysical characteristics are presented in Table 1, are acquired commercially. The hybrid nanofluids composed of GnP-Fe_3O_4/water-ethylene glycol was prepared utilizing the two-step method as given in Fig.1 [19]. Initially, surfactant (SDBS) dissolved in pure water is prepared in three

different ratios based on the precision balance nanoparticle weight values (Figure 2. (e)). Using a mechanical stirrer (Fig. 2 (b)), the base fluid is next treated with GnP-Fe_3O_4 nanoparticles and surfactant solutions to generate nanofluids. To create highly stable hybrid nanofluids, a BANDELIN HD3400 ultrasonic sonicator is used, as shown in Fig. 2(f). After all the nanofluid models are prepared, zeta potential analyses, thermal conductivity, and viscosity measurements are conducted.

2.2 Measurement of thermophysical properties of nanofluid

Before evaluating the thermal conductivity and viscosity of the hybrid nanofluid samples, the samples' stability is assessed using the zeta potential analyzer (Zetasier), as shown in Fig. 3(a). One of the most prominent approaches for assessing the stability of nanofluids is zeta potential analysis. When the zeta potential value is in the ±30 mV region, nanofluids are said to precipitate. Nanofluids having a Zeta potential value of ±0-15 mV exhibit low stability, ±15-30 mV moderate stability, ±30-45 mV high stability, and ±45-60 mV very strong stability [20].

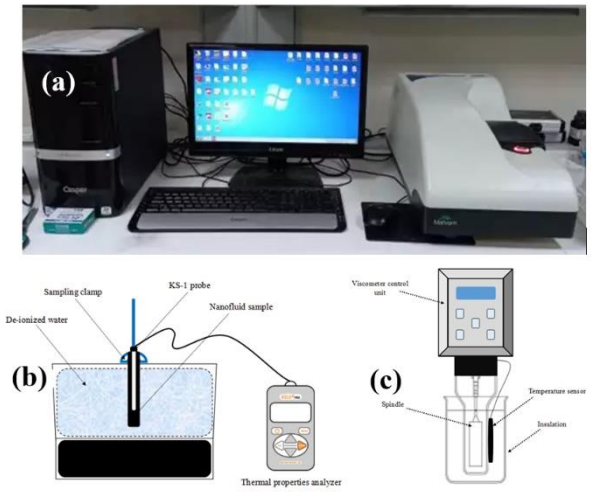

Fig. 3. (a) Zeta potential analyzer, schematics of (b) thermal conductivity and (c) viscosity measurement systems.

Using a thermal conductivity measuring device, the thermal conductivity values of hybrid nanofluid models with various configurations are determined, as shown in Fig. 3(b). The nanofluid sample is heated to the desired temperature using an ultrasonic bath as given in Fig 2(c). The KD2 Pro thermal properties analyser (Fig.2(d)), which measures thermal conductivity, is used in combination with the KS-1 probe. By analysing the mean readings following three repetitions of the measurement, thermal conductivity values are calculated. The dynamic viscosity of hybrid nanofluid samples is measured with a rotational viscometer (Fig. 2(a)). After the calibration of the used spindle that is appropriate for present study viscosity range, a dynamic viscosity measurement set-up is used as given in Fig. 3(c). The nanofluid is spilled into a 100 ml beaker and the measurement is carried out at a rotational speed of 60 rpm under the constant temperature with a measurement accuracy of 1 %. A temperature sensor was used to determine whether the temperature of the nanofluids is at the desired temperature.

2.3 Optimization study parameters and levels

The Taguchi method is an approach to experimental design that is based on analysis of variances (ANOVA) and aims to identify the significant variables influencing experiment variation. The Taguchi technique uses orthogonal arrays for experimental design, which can decrease the quantity of experiments and the amount of work required for each experiment, as well as the time required for each experiment and the signal-to-noise ratios (SNR). Orthogonal arrays are classified according to their factors and levels. One of the most essential aspects of Taguchi analysis is the creation of the orthogonal array type. According to the current research, there are five factors with three levels as given in Table 2. The $L_{27}(3^5)$ type is generated using the Minitab 18.0 software program, as shown in Table 3.

Table 2 Experimental factors and levels

Factors	Levels		
	1	2	3
A-Mechanical stirring(min)	10	20	30
B-Ultrasonic sonication time (min)	30	45	60
C-Ultrasonic sonication power(W)	80	100	120
D-Surfactant fraction(surfactant/nanoparticle)	1/10	2/10	3/10
E-Nanofluid weight fraction(%)	0.5	0.75	1

Table 3 The experimental plan that is created using the $L_{27}(3^5)$ orthogonal array.

Trial	Factors				
	A	B	C	D	E
1	1	1	1	1	1
2	1	1	1	1	2
3	1	1	1	1	3
4	1	2	2	2	1
5	1	2	2	2	2
6	1	2	2	2	3
7	1	3	3	3	1
8	1	3	3	3	2
9	1	3	3	3	3
10	2	1	2	3	1
11	2	1	2	3	2
12	2	1	2	3	3
13	2	2	3	1	1
14	2	2	3	1	2
15	2	2	3	1	3
16	2	3	1	2	1
17	2	3	1	2	2
18	2	3	1	2	3
19	3	1	3	2	1
20	3	1	3	2	2
21	3	1	3	2	3
22	3	2	1	3	1
23	3	2	1	3	2
24	3	2	1	3	3
25	3	3	2	1	1
26	3	3	2	1	2
27	3	3	2	1	3

A performance statistic is used to evaluate the determined characteristics of the objectives (SNR). As opposed to noise, which affects test results but cannot be included in the design of the experiment, signal refers to the actual value in the experiment. Generally speaking, there are three ways to evaluate the SNR: "larger the better," "nominal the better," and "smaller the better"[21,22]. Nanofluids are frequently used in studies aimed at enhancing heat transfer. While they contribute positively to improving heat transfer in thermal systems, they also have an undesired effect of increasing pressure drop. The main approach in this study aims to develop a hybrid fluid model that achieves a relatively higher thermal conductivity, which is a measure of heat transfer capability, while keeping the increase in viscosity, which is the fundamental cause of pressure drop, lower. Therefore, the "larger is better" approach is used in evaluating thermal conductivity, while the "smaller is better" approach is employed in assessing viscosity. The following Eqs. 1 and 2 are employed in this evaluation based on the characteristics.

$$Z_H = -10\log\left(\frac{1}{n}\sum_{i=1}^{n}\frac{1}{Y_i^2}\right) \quad (1)$$

$$Z_L = -10\log\left(\frac{1}{n}\sum_{i=1}^{n}Y_i^2\right) \quad (2)$$

The performance of the i^{th} experiment is denoted by Y, while Z is the value of performance statistics, and n represents the number of repetitions of verification experiments.

3. RESULT

3.1 Taguchi analyses

The Taguchi experimental design method enables simultaneous consideration of multiple factors and delivers the best outcome with the fewest experiments. The experimental study data are then transformed into a signal to noise ratio using the Taguchi technique.

According to the experimental plan that given in Table 3., Table 4. lists the measured thermophysical characteristics of the ethylene glycol-water-based GnP-Fe_3O_4 nanofluid and the SNR values of the parameters.

Table 4 The experimental measurement and SNR values for thermal conductivity and viscosity

Trial	Measurement		SNR	
	Thermal conductivity (W/mK)	Viscosity (kg/ms)	Thermal conductivity (W/mK)	Viscosity (kg/ms)
1	0,5122	0,00160	-5,81121	55,9176
2	0,5173	0,00161	-5,72515	55,8635
3	0,5229	0,00163	-5,63163	55,7562
4	0,5150	0,00154	-5,76386	56,2496
5	0,5173	0,00155	-5,72515	56,1934
6	0,5179	0,00156	-5,71508	56,1375
7	0,5113	0,00141	-5,82648	57,0156
8	0,5126	0,00146	-5,80443	56,7129
9	0,5139	0,00148	-5,78243	56,5948
10	0,5004	0,00151	-6,01365	56,4205
11	0,5014	0,00152	-5,99631	56,3631
12	0,5025	0,00154	-5,97728	56,2496
13	0,5291	0,00157	-5,52924	56,0820
14	0,5262	0,00158	-5,57698	56,0269
15	0,5310	0,00159	-5,49811	55,9721
16	0,5110	0,00152	-5,83158	56,3631
17	0,5230	0,00153	-5,62997	56,3062
18	0,5243	0,00155	-5,60840	56,1934
19	0,5038	0,00156	-5,95484	56,1375
20	0,5158	0,00157	-5,75037	56,0820
21	0,5159	0,00158	-5,74869	56,0269
22	0,5029	0,00151	-5,97037	56,4205
23	0,5082	0,00152	-5,87931	56,3631
24	0,5095	0,00153	-5,85712	56,3062
25	0,5343	0,00156	-5,44430	56,1375
26	0,5331	0,00158	-5,46383	56,0269
27	0,5318	0,00160	-5,48503	55,9176

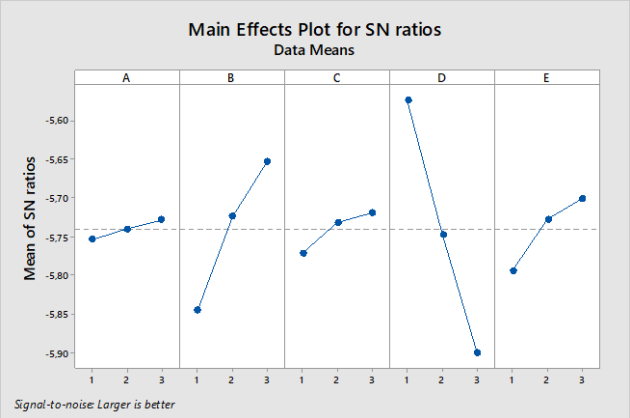

Fig. 4. The mean of SNRs for thermal conductivity.

Fig 4. shows the mean of SNRs for thermal conductivity. The SNR values of mechanical stirring, ultrasonic sonication time and power, and nanofluid weight fraction progress an increment trend with risen level of each parameter. On the contrary, the SNR values tend to decrease with the use of higher fraction of surfactant as in Fig. 4.

Table 5 Average SNR values for thermal conductivity

Factors	Levels		
	1	2	3
A	-5,75	-5,74	**-5,73**
B	-5,85	-5,72	**-5,65**
C	-5,77	-5,73	**-5,72**
D	**-5,57**	-5,75	-5,90
E	-5,79	-5,73	**-5,70**

Mean=-5,74 dB

***Optimum level**

Table 5 summarizes the average SNR values for factors with a variety of levels. The obtained findings indicate that, the highest SNR value of -5.57 dB is confirmed for factor D (surfactant fraction) at the lowest level of 1/10, while the lowest SNR of -5.90 dB is determined for the highest level of 3/10. The highest SNR values for thermal conductivity are obtained with the highest levels of mechanical stirring, ultrasonic sonication time and power, and nanofluid weight

fraction. As given in Table 5. the configuration of A3B3C3D1E3 shows the best SNR values or thermal conductivity.

Fig. 5. demonstrates the average SNR distribution versus variety parameters and levels. The acquired data show that the surfactant ratio has the greatest impact on the range of SNR distribution for viscosity; besides, the SNR values tend to rise with ascending of ultrasonic sonication and time, and the surfactant fraction.

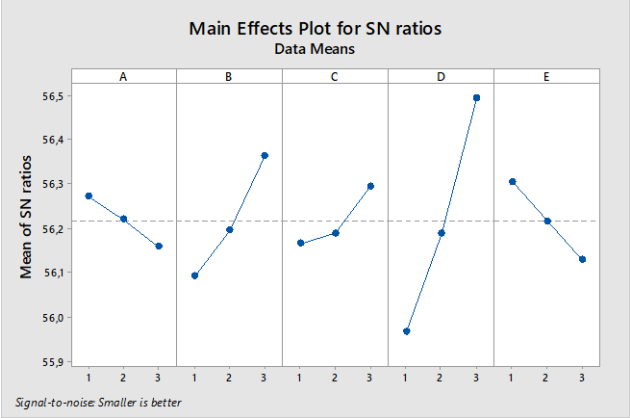

Fig. 5. The mean of SNRs for viscosity.

Table 6 Average SNR values for viscosity

Factors	Levels		
	1	**2**	**3**
A	**56,27**	56,22	56,16
B	56,09	56,19	**56,36**
C	56,17	56,19	**56,29**
D	55,97	56,19	**56,49**
E	**56,30**	56,22	56,13

Mean=56,22 dB

***Optimum level**

As can be understood from Table 6, the surfactant fraction is the most effective parameter on viscosity as well as thermal conductivity. While the highest SNR value is obtained at the highest level of this factor, the lowest SNR value is also obtained at the lowest level of the surfactant fraction factor. The highest level of ultrasonic sonication time and power, and surfactant fraction also achieve the highest SNR for viscosity. The optimum configuration for viscosity is determined as A1B3C3D3E1, with an average SNR of 56.22 dB obtained from all factors and levels.

3.2 ANOVA approach

The Taguchi technique is based on the analysis of variance (ANOVA), which is used when comparing two or more independent groups. In the current study, the influence of five independent factors on the thermal conductivity and viscosity of hybrid nanofluid is examined; as a result, an ANOVA is used to calculate the effect rates of the independent parameters.

The results of the ANOVA for the effects of thermal conductivity by the applied variables and levels are shown in Table 7. Accordingly, the contributions are as follows in order of importance: surfactant fraction, ultrasonic sonication time, nanofluid weight fraction, and ultrasonic sonication power and mechanical stirring. Table 7 shows that the surfactant fraction, which has a 63.57% contribution rate, is the most effective parameter.

As shown in Figure 6, ultrasonic sonication time provides the second highest and the nanofluid weight fraction provides the third highest contribution to thermal conductivity with 23.53% and 5.49%, respectively, while mechanical stirring provides the lowest contribution with 0.39%.

Table 7 ANOVA results for thermal conductivity

Factors	DF	Seq SS	Contribution	Adj SS	Adj MS	F-Test
A	2	0,002984	0,39%	0,002984	0,001492	0,51
B	2	0,170625	25,53%	0,170625	0,085312	28,98
C	2	0,01357	1,79%	0,01357	0,006785	2,3
D	2	0,48144	63,57%	0,48144	0,24072	81,76
E	2	0,041585	5,49%	0,041585	0,020793	7,06
Error	16	0,047106	0,02%	0,047106	0,002944	
Total	26	0,757311	100,00%			

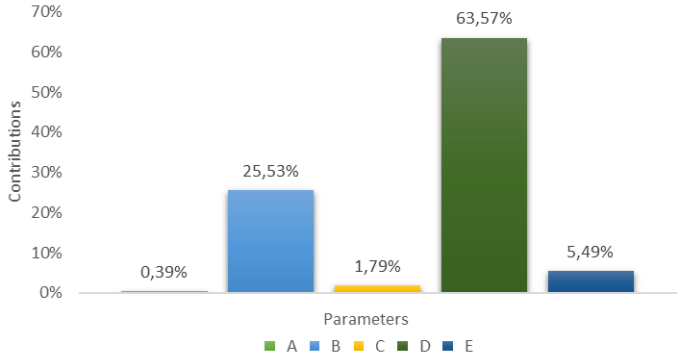

Fig. 6. The contribution rate for thermal conductivity.

Table 8 ANOVA results for viscosity

Factors	DF	Seq SS	Contribution	Adj SS	Adj MS	F-Test
A	2	0,05831	3,02%	0,05831	0,029154	10,03
B	2	0,34005	17,59%	0,34005	0,170025	58,47
C	2	0,08526	4,41%	0,08526	0,04263	14,66
D	2	1,26229	65,31%	1,26229	0,631146	217,06
E	2	0,14041	7,26%	0,14041	0,070204	24,14
Error	16	0,04652	2,41%	0,04652	0,002908	
Total	26	1,93284	100,00%			

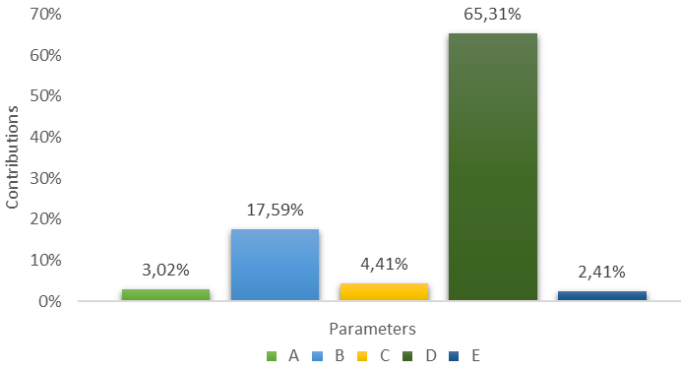

Fig. 7. The contribution rate for viscosity.

As listed in Table 8, the surfactant fraction shows the greatest contribution with 65.31% on viscosity, followed by ultrasonic sonication time at 17.59%, which is similar to the findings for thermal conductivity. The nanofluid weight fraction provides the lowest, followed by mechanical stirring with the second-lowest contribution, and ultrasonic sonication power with the third-lowest contribution order, according to an evaluation of the contribution rates shown in Figure 7.

As evidenced by the findings of the study, the utilization of nanoparticles exhibits a pronounced influence on thermal conductivity while demonstrating a comparatively lesser impact on viscosity. These outcomes are consistent with the research conducted by Wohld et al.[23]. Furthermore, Mane and Hemadri [24] emphasized in their ANOVA results that the $CuO+Fe_3O_4$ nanofluid contributed the highest enhancement to thermal conductivity, consistent with the findings of this study, highlighting the role of surfactant utilization. Lastly, Karmare et al.[] stated that particle loading is a significant factor influencing both viscosity and thermal conductivity, aligning with the results of our study.

4. CONCLUSION

The effects of varying the mechanical stirring, ultrasonic sonification time and power, surfactant fraction, and nanofluid weight fraction on the thermal conductivity and viscosity of a binary hybrid GnP-Fe_3O_4/ethylene glycol-water nanofluid are taken into account in the current research. The viscosity and thermal conductivity are optimized with a single objective in consideration. The effects of each parameter are also evaluated using ANOVA. The findings are as follows:

- In single-objective optimization, the highest level of factors A, B, C and E produces the highest SNR values for thermal conductivity, while the lowest level of D factor provides the highest SNR value. For viscosity, maximum SNR values are determined at the lowest levels of factors A and E, and at the highest levels of factors B, C and D.
- It is concluded that the optimum experimental variation for thermal conductivity is A3B3C3D1E3, while for viscosity the optimum variation is A1B3C3D3E1.
- For thermal conductivity, the most significant factors are surfactant fraction, ultrasonic sonication time, nanofluid weight fraction, ultrasonic sonication power, and mechanical mixing; for viscosity, the factors are surfactant fraction, ultrasonic sonication time, ultrasonic sonication power, mechanical mixing, and nanofluid weight ratio.
- ANOVA approach determines that the highest contribution for both thermophysical properties is provided by the surfactant fraction, such a result contributes to the fact that it is more possible to determine the thermophysical properties of stable nanofluids.

Acknowledgments

The authors would like to express their gratitude to TUBITAK for providing financial support for the project identified 221M687.

REFERENCES

[1] C. Şimşek, S.O. Akansu, Numerical Investigation of The Effect of Finned Obstacle on Heat Transfer Characteristics in a Rectangular Channel, *Energy, Environment and Storage*, 01, 1-6, 2021.

[2] S. Ünalan, E. Özrahat, Numerical Investigation of the Effects of Window Height and Gas Thickness on Heat Transfer and Gas Flow in Double Pane Windows, *Energy, Environment and Storage*, 01, 13-25, 2021.

[3] R. Agarwal, P. Rawat, D. Rai, H. Athar, S. Naik, Phase Change Materials for Energy Efficiency in Building Components–Overview, *Energy, Environment and Storage*, 02, 23-29, 2022.

[4] A. Karabey, S. Arvasi Optimization of the Design Parameters Using the Taguchi method in Inclined Impingement Multijet Heat Transfer with Rectangular Finned Heat Sink, Heat Transfer Research, 54, 67-51, 2023.

[5] J. Sarkar, P. Ghosh, A. Adil, A review on hybrid nanofluids: recent research development and applications, *Renewable and Sustainable Energy Reviews*. 43, 164–177, 2015.

[6] TS. Krishnakumar, SP. Viswanath, SM. Varghese, JM. Prakash, Experimental thermal studies on and rheological properties of Al2O3–ethylene glycol nanofluid. *International Journal of Refrigeration*, 2018(89),122–130.

[7] X. Su, M. Zhang, X. Guo, Enhancement of Transport in Oscillating Heat Pipe with Ternary Fluid, *International Journal of Heat and Mass Transfer*, 87(8),258–264, 2015.

[8] T. Elnaqeeb, I. Animasaun, N. Shah , Ternary-hybrid nanofluids, significance of suction and dual-stretching on three-dimensional flow of water conveying nanoparticles with various shapes and densities, *Zeitschrift für Naturforschung A*, 76(3),231-243, 2021.

[9] D. Toghraie, VA. Chaharsoghi, M. Afrand, Measurement of thermal conductivity of ZnO–TiO2/EG hybrid nanofluid effects of temperature and nanoparticles concentration, *Journal of Thermal Analysis and Calorimetry*, 125, 527-535, 2016.

[10] S. Suresh, KP. Venkitaraj, P. Selvakumar, M. Chandrasekar, Synthesis of Al2O3–Cu/water hybrid nanofluids using two step method and its thermo physical properties, *Colloids and Surfaces A: Physicochemical and Engineering Aspects*, 388(1),41-48, 2011.

[11] Y. Liu, D. Yin, M. Tian, X. Hu, X. Chen, Experimental investigation on the viscosity of hybrid nanofluids made of two kinds of nanoparticles mixed in engine oil, *Micro Nano Letters*, 13,1197-1202, 2018.

[12] M. Hemmat Esfe, S. Wongwises, A. Nader, A. Asadi, M.R. Safaei, H. Rostamian, M. Dahari, A. Karimipous, Thermal conductivity of Cu/TiO2–water/EG

hybrid nanofluid: Experimental data and modeling using artificial neural network and correlation, *International Communications in Heat and Mass Transfer*, 66, 100-104, 2015.

[13] O. Soltani, M. Akbari, Effects of temperature and particles concentration on the dynamic viscosity of MgO-MWCNT/ethylene glycol hybrid nanofluid, *Experimental study, Physica E: Low-dimensional Systems and Nanostructures*, 87,564-570, 2016.

[14] M. I. H. C. Abdullah, A. Othman, R. Abdullah, and M. F. Abdollah, Optimization on the Nanoparticles Stability in Liquid Phased Condition by Using Taguchi Analysis, *Journal of Advanced Research in Fluid Mechanics and Thermal Sciences*, 61,140–150, 2019.

[15] J. Rubasingh, P. Selvakumar, Enabling Taguchi method with grey relational analysis to optimize the parameters of TiO2/ZnO heat transfer nanofluid for heat pipe application, *Nano Express*,2, 010034, 2021.

[16] R. Choudhary, N. Sharma, S. Subudhi, A Taguchi approach for optimization of design parameters on Rayleigh-Bénard convection in water-based Al2O3 nanofluids, *World Journal of Engineering*, 19(3),375-380, 2022.

[17] S. Ravi Babu, G. Sambasiva Rao, Experimental Investigation of Natural Convective Heat Transfer Using Water-Alumina Nanofluid with Taguchi Design of Experiments, *International Journal of Mechanical Engineering and Technology*, 8(7), 795–804, 2017.

[18] Nanografi Inc., Nanoparticles https://www.nanografi.com.tr/ (accessed 28 September 2022)

[19] S Z. Said, N.K. Cakmak, P. Sharma, L.S. Sundar, A. Inayat, O. Keklikcioglu, C. Li, Synthesis, stability, density, viscosity of ethylene glycol-based ternary hybrid nanofluids: Experimental investigations and model - prediction using modern machine learning techniques, *Powder Technology*, 400, 117190, 2022.

[20] T. Dagdevir, V. Ozceyhan, Optimization of process parameters in terms of stabilization and thermal conductivity on water based TiO2 nanofluid preparation by using Taguchi method and Grey relation analysis, *International Communications in Heat and Mass Transfer*,120,105047,2021.

[21] S. Güneş, E. Şenyiğit, E. Karakaya, V. Özceyhan, Optimization of heat transfer and pressure drop in a tube with loose-fit perforated twisted tapes by Taguchi method and grey relational analysis, J*ournal of Thermal Analysis and Calorimetry*, 136,1795-1806,2019.

[22] E. Şenyiğit, B. Demirel, Material selection on countermeasure flares systems by multi criteria decision making methods, *International Journal of Multidisciplinary Studies and Innovative Technologies*, 4, 1-9, 2020.

[23] J. Wohld, J. Beck, K. Inman, M. Palmer, M. Cummings, R. Fulmer, S. Vafaei, Hybrid Nanofluid Thermal Conductivity and Optimization: Original Approach and Background, *Nanomaterials*, 12, 2847,2022.

[24] N. S. Mane, V. Hemadri, Study of the effect of preparation parameters on thermal conductivity of metal oxide nanofluids using Taguchi method, J*ournal of Energy Systems*, 5(2), 149-164, 2021.

[25] S. Karmare, P. Patil, K. Deshmukh et al. Prediction and Optimization of Thermal Conductivity and Viscosity of Stable Plasmonic TiN Nanofluid Using Response Surface Method For Solar Thermal Application, 15 September 2022, PREPRINT (Version 1) available at Research Square [https://doi.org/10.21203/rs.3.rs-2057883/v1]

Research Article

Energy, Environment and Storage (2023)03-02:66-69

Energy, Environment and Storage

Journal Homepage: www.enenstrg.com

Deep Eutectic Solvents for Liquid-Liquid Extraction-Denitrification

Sayad Niftullayeva[1*], Yegana Mamedova [2], Ibrahim Mamedov [3*]

[1] Baku State University, Baku, Azerbaijan, ORCID: 0000-0002-5757-9899
Baku State University, Faculty of Chemistry, Z. Khalilov 23, Baku, Azerbaijan
Correspondence Author: Ibrahim Mamedov, Baku State University, Baku, Azerbaijan
email: bsu.nmrlab@gmail.com, phone: +994 12 5382106

ABSTRACT. In this study, a new type of deep eutectic solvent was prepared and tested for the selective extraction of nitrogen compounds from model fuels. DES2 was made of triethylammonium acetate $[TEA]^+[AcO]^-$ and glycerol in a volume ratio of 1:6. The extraction capacity of DES2 was evaluated and compared to DES1a, and DES1b. The denitrification process was carried out at room temperature. The volume ratio of DESs to model fuels were taken 1:1. Obtained results showed, that DES2 was highly selective for all nitrogen compounds (pyridine, quinoline, indole, and pyridine/quinoline mixture) in a one-step liquid-liquid extraction (LLE). The purification rate of the pyridine, indole and pyridine/quinoline mixture was 100, 98 and 88% in one hour. Quinoline showed high-extraction efficiency (92%) in three hours of mixing time. All experiments were evaluated by NMR spectra.

Keywords: DES, denitrification, NMR, glycerol, separation

Article History: Received: 08.04.2023; Accepted:20.04.2023; Available Online: 29.05.2023
Doi: https://doi.org/10.52924/SGAW3909

The abbreviations:

DESs -Deep eutectic solvents
DES1a - NH_4Cl:Glycerol (1:12)
DES1b - NH_4Cl:Glycerol (1:6)
DES2 - Triethylammonium acetate:Glycerol (1:6)
$[TEA]^+[AcO]^-$ -triethylammonium acetate
HBD -hydrogen bond donor
HBA -hydrogen bond acceptor
LLE -liquid-liquid extraction

1. INTRODUCTION

The fundamental principles of green chemistry aim to design less consumption of energy, use non-toxic chemical reagents, decrease environmental pollution, and include waste prevention [1]. For this reason, new types of green solvents called ionic liquids, invested as alternatives to classical organic solvents. ILs have been widely used due to their remarkable properties such as high thermal stability, low vapor pressure, nonflammability, recycling, etc[2-4]. However, some disadvantages of ILs limited their application. The poor biodegradability, toxicity, complexity, and highly costly synthesis are considerable drawbacks to the use of these solvents [5].

Deep eutectic solvents, analogs to ionic liquids have emerged as a new generation of eco-friendly solvents. DESs are typically easy to synthesize. It is prepared by

The current work reports the selective separation of nitrogen compounds with a new deep eutectic solvent DES2. Pyridine, quinoline, indole, and pyridine/quinoline mixture with 1,7% were the content of model fuel (mixtures of n-decane and n-hexadecane). The purification of model fuels by DESs was investigated and evaluated at room temperature.

The results showed the extraction capacity of DES2 was higher than DES1a and DES1b for all nitrogen components. For the pyridine, quinoline, indole, and pyridine/quinoline mixtures high results were obtained in 1 hour by DES2. The experiments were evaluated by ^1H NMR analysis.

2. EXPERIMENTAL

2.1 Materials and methods

Chemicals
All chemicals used in this paper were obtained from Sigma-Aldrich (Germany). Pyridine, quinoline, and indole with ≥ 99% high purity were used to prepare new model

*Corresponding author: bsu.nmrlab@gmail.com

fuel samples. Triethylammonium acetate $[TEA]^+[AcO]^-$ was synthesized in the laboratory.

Synthesis of DESs

DES2 was synthesized by mixing triethylammonium acetate $[TEA]^+[AcO]^-$ as a hydrogen bond acceptor and glycerol as a hydrogen bond donor. The volume ratio of HBA:HBD was taken 1:6.

Experimental procedure

Pyridine, quinoline, pyridine/quinoline and indole with 1,7% content were added to the mixture of n-decane and hexadecane (model fuel). LLE process was investigated in a volume ratio of DESs to model fuels 1:1. All experiments were carried out at room temperature (Figure 1 and 2).

Fig. 1. Preparation of the DES2

Fig. 2. LLE of nitrogen compounds from the model fuel

NMR analysis

LLE evaluation was by the integral intensity of 1H NMR spectra. NMR experiments have been performed on a BRUKER FT NMR spectrometer (UltraShieldTM Magnet) AVANCE 300 (300.130 MHz) with a BVT 3200 variable temperature unit in 5 mm sample tubes using Bruker Standard software (TopSpin 3.1). The ^1H chemical shifts were referenced to internal tetramethylsilane (TMS); the experimental parameters for ^1H: digital resolution = 0.23 Hz, SWH = 7530 Hz, TD = 32 K, SI = 16 K, 90^0 pulse-length = 10 µs, PL1 = 3 dB, ns-= 1, ds= 0, d1 =1 s; for ^{13}C: digital resolution = 0.27 Hz, SWH = 17985 Hz, TD = 64 K, SI = 32 K, 90^0 pulse-length = 9 µs, PL1 = 1.5 dB, ns= 100, ds= 2, d1= 3 s. NMR-grade $CDCl_3$ was used for the analysis of model fuel blends.

3. RESULTS AND DISCUSSION

3.1 Characterization of DESs

Some physical properties of DESs have shown in Table 1. The value of solvent viscosity and density are considerable factors for the separation process. The energy consumption of the mixing process and the mixing regime is determined due to viscosity and density. On the other side, the rate of stratification also depends on the solvent density [17].

Table 1 Some physical properties of DESs

Type of DES (HBA: HBD)	Density at 20° C, g/sm^3	Viscosity, at 20°C, mm²/s	Viscosity, at 40°C, mm²/s
DES 1a	**1,2307**	**97,384**	**32,647**
DES 1b	**1,2309**	**81,656**	**27,829**
DES 2	**1,1949**	**120,812**	**36,780**

In addition, the stability data was tested at 298,15 K, 1 atm. over a month. All DESs showed high results and remained as homogenous liquid at room temperature.

3.2. Liquid-liquid extraction process

From our previous research, it is obvious that DES1a and DES1b were checked for the selective extraction of pyridine, quinoline, indole and pyridine/quinoline mixture. In this work, we studied the separation of all indicated nitrogen compounds by DES2, based on triethylammonium acetate $[TEA]^+[AcO]^-$ and the selectivity compared to DES1a and DES1b. All experiments were carried out at room temperature.

As can be seen from Table 2 and Table 3, the optimal separation efficiencies of indole were observed in 3 hours of mixing time. DES1b (94%) was more selective than DES1a (80%) in the same molar ratio and reaction conditions. However, in three hours of mixing time, the maximum separation results of quinoline were 60% by DES1a and 50% by DES1b.

Pyridine was completely separated in one hour of mixing time by DES1b. The pyridine/quinoline mixture was purified from the model fuel in one-hour mixing time by DES1a. The high extraction efficiency was 72%.

Table 2 Extraction of nitrogen compounds by DES1a at room temperature

DES [NH_4Cl (1): Glycerol (12)]			
Amount of nitrogen compounds	**DES: fuel (volume ratio)**	**Time (hour)**	**Separation efficiency, (%)**
Pyridine (1,7%)	1:1	1	87
Pyridine (1,7%)	1:1	3	92
Pyridine (1,7%)	1:1	5	85
Indole (1,7%)	1:1	1	38
Indole (1,7%)	1:1	3	80
Indole (1,7%)	1:1	5	71
Quinoline (1,7%)	1:1	1	40
Quinoline (1,7%)	1:1	3	60
Quinoline (1,7%)	1:1	5	46
Pyridine/Quinoline (1,7%)	1:1	1	72
Pyridine/Quinoline (1,7%)	1:1	3	58
Pyridine/Quinoline (1,7%)	1:1	5	45

Table 3 Extraction of nitrogen compounds by DES1b at room temperature

DES [NH_4Cl (1): Glycerol (6)]			
Amount of nitrogen compounds	**DES: fuel (volume ratio)**	**Time (hour)**	**Separation efficiency, (%)**
Pyridine (1,7%)	1:1	1	100
Pyridine (1,7%)	1:1	3	91
Pyridine (1,7%)	1:1	5	85
Indole (1,7%)	1:1	1	49
Indole (1,7%)	1:1	3	94
Indole (1,7%)	1:1	5	88
Quinoline (1,7%)	1:1	1	42
Quinoline (1,7%)	1:1	3	50
Quinoline (1,7%)	1:1	5	43
Pyridine/Quinoline (1,7%)	1:1	1	62
Pyridine/Quinoline (1,7%)	1:1	3	55
Pyridine/Quinoline (1,7%)	1:1	5	48

The extraction capacity of DES2 for each nitrogen component was listed in Table 4. NMR analysis for pyridine, quinoline, indole, and pyridine/quinoline mixture showed, that high results were in 1 hour mixing time. Pyridine was completely separated from model fuel (Figure 3). The purification rate of the indole and pyridine/quinoline mixture was 98% and 88%. Quinoline showed high-extraction efficiency in three hours of mixing time. We could receive 92% separation at a single-stage LLE.

Table 4 Extraction of nitrogen compounds by DES2 at room temperature

DES [triethylammonium acetate (1): Glycerol (6)]			
Amount of nitrogen compounds	**DES: fuel (volume ratio)**	**Time (hour)**	**Separation efficiency, (%)**
Pyridine (1,7%)	1:1	1	100
Pyridine (1,7%)	1:1	3	94
Pyridine (1,7%)	1:1	5	83
Indole (1,7%)	1:1	1	98
Indole (1,7%)	1:1	3	86
Indole (1,7%)	1:1	5	73
Quinoline (1,7%)	1:1	1	81
Quinoline (1,7%)	1:1	3	92
Quinoline (1,7%)	1:1	5	59
Pyridine/Quinoline (1,7%)	1:1	1	88
Pyridine/Quinoline (1,7%)	1:1	3	63
Pyridine/Quinoline (1,7%)	1:1	5	51

It is also evident from Scheme 1, DES2 is more selective for the denitrification process than DES1a and DES1b. In one hour of mixing time, DES2 showed very high extraction for each nitrogen compound. The separation efficiency decreased linearly with increasing mixing time for the pyridine, indole, and pyridine/quinoline mixture. In contrast to other compounds, the best result for quinoline was reached in three hours of mixing time by DES2. DESs can be ranked according to the ability of removing nitrogen compounds from model fuel like that: *DES1a<DES1b<DES2*.

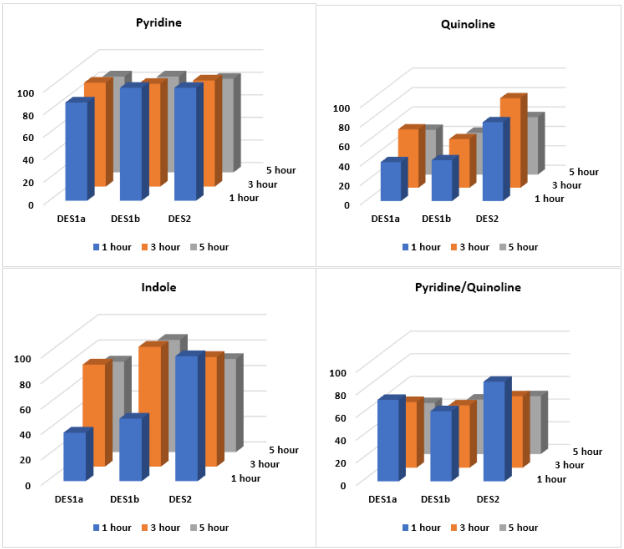

Scheme 1. The separation efficiency of nitrogen compounds by DES1a, DES1b, and DES2

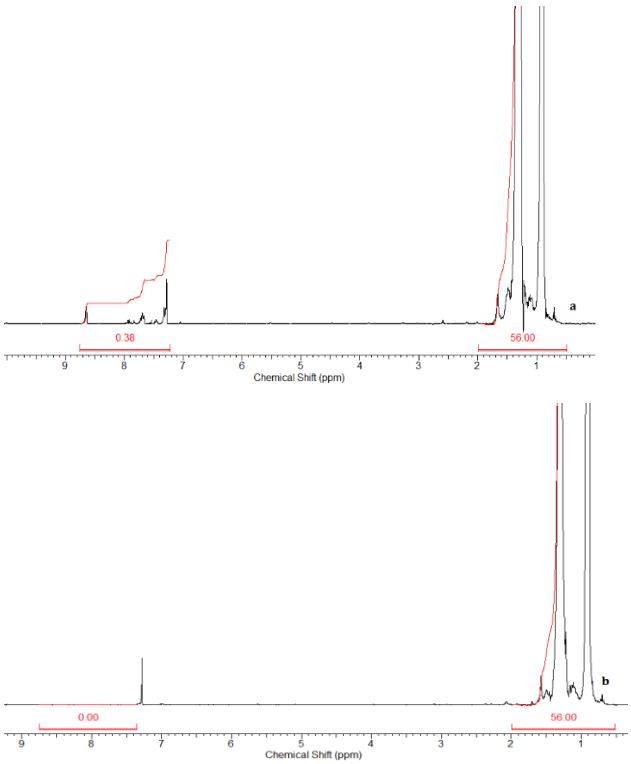

Fig. 3. ^{1}H NMR analysis for pyridine of before (***a***) and after (***b***) LLE

4. CONCLUSION

In this study, we investigated the selectivity of a new type of deep eutectic solvent for the separation of nitrogen compounds from model fuel. DES2 was synthesized by mixing triethylammonium acetate as HBA and glycerol as HBD. The denitrification process was carried out at room temperature, and the results were compared between DES1a, DES1b, and DES2. From the obtained results, it is obvious that DES2 is more selective for all nitrogen components. In one hour of mixing, the maximum separation efficiencies of the indole and pyridine/quinoline mixture were 98% and 88%, respectively, by using DES2. High-efficiency separation for quinoline was 92% in three hours of mixing time. Pyridine was completely separated from model fuel at a single-stage LLE by DES1b and DES2. DES1a showed a lower selectivity capacity for the most of nitrogen components than DES1b and DES2.

REFERENCES

[1] Anastas, P.T., Warner, J.C. Principles of green chemistry. *Green chemistry: Theory and practice*, 1998, 135p.

[2] Ghandi, K. A review of ionic liquids, their limits and applications. *Green and sustainable chemistry*, 4, 44-53, 2014.

[3] Walkoli, A.T., Sonawane, P.D. Ionic liquids: Eco-friendly solvent, *Research & Reviews in Biotechnology & Biosciences*, 9(1), 9-13, 2022.

[4] Welton, T. Room-temperature ionic liquids. Solvents for synthesis and catalysis, *Chemical reviews*, 99(8), 2071-2084, 1999.

[5] Peric, B., Sierra, J., Martí, E., Cruañas, R., Garau, M.A, Arning, J., Bottin-Weber, U., Stolte, S. (Eco) toxicity and biodegradability of selected protic and aprotic ionic liquids, *Journal of hazardous materials*, 261, 99-105, 2013.

[6] Zhang, Q., Vigier, K.D., Royer, S., Jérôme, F. Deep eutectic solvents: syntheses, properties and applications, *Chemical Society Reviews*, 41(21), 7108-7146, 2012.

[7] Abbott, A.P., Boothby, D., Capper, G., Davies, D.L., Rasheed, R.K. Deep eutectic solvents formed between choline chloride and carboxylic acids: versatile alternatives to ionic liquids, *Journal of the American Chemical Society*, 126(29), 9142-9147, 2004.

[8] Hansen, B.B., Spittle, S., Chen, B., Poe, D., Zhang, Y., Klein, J.M., Horton, A., Adhikari, L., Zelovich, T., Doherty, B.W., Gurkan, B. Deep eutectic solvents: A review of fundamentals and applications, *Chemical reviews*, 121(3), 1232-1285, 2020.

[9] Elachkar, T., Greige-Gerges, H., Fourmentin, S. Basics and properties of deep eutectic solvents: a review, *Environmental chemistry letters*, 19, 3397-3408, 2021.

[10] Tang, B., Row, K.H. Recent developments in deep eutectic solvents in chemical sciences. *Monatshefte für Chemie-Chemical Monthly*, 144, 1427-1454, 2013.

[11] Chen, J., Li, Y., Wang, X., Liu, W. Application of deep eutectic solvents in food analysis: A review, *Molecules*, 24(24), 4594-4604, 2019.

[12] Shahbaz, K., Mjalli, F.S., Hashim, M.A., Alnashef, I.M. Using deep eutectic solvents based on methyl triphenyl phosphunium bromide for the removal of glycerol from palm-oil-based biodiesel, *Energy & Fuels*, 25(6), 2671-2678, 2011.

[13] Warrag, S.E., Darwish, A.S., Abuhatab, F.O., Adeyemi, I.A., Kroon, M.C., Alnashef, I.M. Combined extractive dearomatization, desulfurization, and denitrogenation of oil fuels using deep eutectic solvents: A parametric study, *Industrial & Engineering Chemistry Research*, 59(25), 11723-11733, 2020.

[14] Warrag, S.E., Darwish, A.S., Adeyemi, I.A., Hadj-Kali, M.K., Kroon, M.C., Alnashef I.M. Extraction of pyridine from n-alkane mixtures using methyltriphenylphosphonium bromide-based deep eutectic solvents as extractive denitrogenation agents, *Fluid Phase Equilibria*, 517, 112622, 2020.

[15] Sudhir, N., Yadav, P., Nautiya,l B.R., Singh, R., Rastogi, H., Chauhan, H. Extractive desulfurization of fuel with methyltriphenyl phosphonium bromide-tetraethylene glycol-based eutectic solvents, *Separation Science and Technology*, 55(3), 554-563, 2020.

[16] Niftullayeva, S., Mamedov, I. Extraction of nitrogen compounds from model fuel by DES,

Modern problems of theoretical & experimental chemistry, *International conference*, 168-169, 2022.

[17] Rogošić, M., Kučan, K.Z. Deep eutectic solvent based on choline chloride and propylene glycol as a potential medium for extraction denitrification of hydrocarbon fuels, *Chemical Engineering Research and Design*, 161, 45-57, 2020.

Research Article *Energy, Environment and Storage* (2023)03-02:70-80

Energy, Environment and Storage

Journal Homepage: www.enenstrg.com

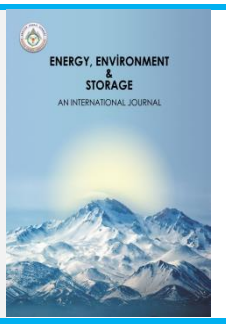

A Comparison of Energy Use in Conventional and Organic Olive Production in Kaz Mountains, Çanakkale, Türkiye

Hatice Dal[1,2], Evrim Karaçetin[3]*

[1] *İzmir Kavram Vocational School, Department of Medical Services and Techniques, Environmental Health Program, İzmir, Turkey ORCID: 0000-0002-6220-8339*
[2]*Erciyes University, Engineering Faculty, Environmental Engineering Department, Kayseri, Turkey, ORCID: 0000-0002-6220-8339*
[3]*Erciyes University, Engineering Faculty, Environmental Engineering Department, Kayseri, Turkey, ORCID: 0000-0002-7311-1989*

ABSTRACT. Agriculture is one of the biggest sectors and energy consumption during agricultural production causes a release of 11 % of greenhouse gasses leading to climate change. Since after the industrialization of agriculture, farming systems shifted towards high-intensity farming, yet in Türkiye, traditional farming methods continue. In this study we compare the energy efficiency of organic vs. conventional olive groves in Kaz Mountains, Türkiye. 71 farmers were interviewed face-to-face in two subsequent years and the energy efficiency of the olive production process was calculated as the ratio of the energy spent during farming to the energy content of the fruit. Fuel use was calculated under the direct energy input, whereas production processes of fertilizer, agricultural machinery, maintenance and repair, human and animal labor were calculated under indirect energy inputs. Here we show that conventional olive production was less energy efficient due to the high indirect energy input during the production of synthetic fertilizers. There was no relationship between the energy input and yield. This study shows that by improving energy efficiency, the technical performance of agricultural systems can be increased and their negative impact on the environment can be reduced.

Keywords: Olive Production, Energy Efficiency, Energy Consumption, Organic Farming, Conventional Farming

Article History: Received:28.04.2023; Accepted:11.05.2023; Available Online: 29.05.2023
Doi: https://doi.org/10.52924/XEHC9087

1. INTRODUCTION

Olive production in Türkiye has developed rapidly since 1937. Traditional olive production generally involves building stone terraces along slopes in shallow fertile soil type [1] where main energy is human and animal power with lack of chemical input. Although profound changes have been made in the practices in olive groves while low-density systems are replaced by high-density farms [2], in Türkiye many olive groves continue produce olive with traditional farming methods while adding the use of synthetic fertilizers and pesticides, a very broad farming method defined as conventional farming. Yet, due to the environmental impacts of pesticide use in conventional farming, and with the increase of awareness among farmers and consumers, organic farming, an agricultural method where synthetic inputs are banned, has gained more importance. The demand for products produced by organic methods has gradually increased and organic product markets have developed rapidly [3].

Conventional and organic farming have differences in applications, one of the most prominent differences is the ban of synthetic chemical use in organic farming. Yet, except this difference there also are many similarities such as the use of fossil fuel, agricultural machinery, irrigation methods. Mechanization is one factor increasing the energy demand and use and due to this fact energy consumption in the agricultural sector is increasing rapidly [4]. Energy consumption in turn, causes environmental problems such as global warming, air pollution, acid rain and ozone depletion [5]. To ensure a sustainable development in the agricultural sector, it is essential to increase energy efficiency and as the concept of sustainable development gains more and more importance, the efforts towards energy efficiency are also becoming important. For this purpose, improving energy efficiency during all stages, preventing waste, reducing energy loss both on sectoral and macro level are among the priority actions [4]. If energy efficiency can be improved, the technical performance of the agricultural system will increase, while the damage to the environment will be reduced. Increasing energy efficiency will contribute economically to producers as well as reducing environmental impacts [6].

Many studies have been carried out in different countries on the energy efficiency of olive groves. The energy

*Corresponding author: ekaracetin@erciyes.edu.tr

efficiency of olive groves in Greece [3, 7, 8], Italy [9, 10], Spain [11], Morocco and Portugal [12] were previously studied. In Türkiye, the research in this area is very limited. Hence it is important to compare different production methods and determine the most suitable methods to reduce energy use without causing a decrease in the yield in order to reduce the negative effects of agriculture on the environment.

This study concentrates on olive farms to compare the energy efficiency and yield between conventional and organic olive groves in Kaz Mountains, Çanakkale, Türkiye. Two questions were answered "Which farming type uses more energy, organic or conventional?" and "Which farming type is more energy efficient?". This paper also tries to answer if small adjustments in each farming methods can be made to decrease the environmental impacts and increase the energy efficiency of olive production.

2. MATERIALS AND METHODS

2.1 Study Area

One of the leading regions in olive cultivation in Turkey is the Marmara Region, where Türkiye realizes 18% of its total olive production [13, 14]. In Çanakkale, 9.6% of the agricultural lands are covered with olive groves and Turkey meets 7.3% of its olive production from Çanakkale [15]. Olive groves are more concentrated in the coastal parts of Ayvacık and Ezine districts. About 1,734,000 of the 4,107,000 olive trees in the province belong to Ayvacık districts [16].

The study was carried out in olive groves in Kaz Mountains, north of Edremit Bay, between Balıkesir and Çanakkale provinces in the Marmara Region (Fig. 1). Kaz Mountains are located between 26°15′-26°35′ east longitudes and 39°30′-39°50′ north latitudes. The region is surrounded by Ayvacık and Ezine provinces in the west, Bayramiç and Çan in the north, Kalkım, Yenice and Balya in the east, and Edremit and Havran in the south [17].

Fig. 1. The study area (Red color: Organic farms, blue: conventional farms, green: natural areas).

The olive groves are located both on slope and flat areas and the climate has both the characteristics of the Central Anatolia and the Mediterranean Regions [17]. While the annual precipitation ranges between 579.1 mm and 844.3 mm, the annual average relative humidity varies between 60% and 74%, and the annual average temperature between 12.8 ℃ and 13.2 ℃ [18].

2.2 Aim and Scope

The aim of this study is to determine if energy efficiency differs between conventional and organic olive production systems in Kaz Mountains. agricultural activities will be recommended.

Two different olive groves, organic and conventional, were studied in Kaz Mountains. Fig. 2 shows the system boundaries of organic and conventional olive groves. In organic areas, it is allowed to use burgundy slurry (a mixture of copper (II) sulfate and slaked lime) authorized by the EU to combat fungal disease on olive trees.

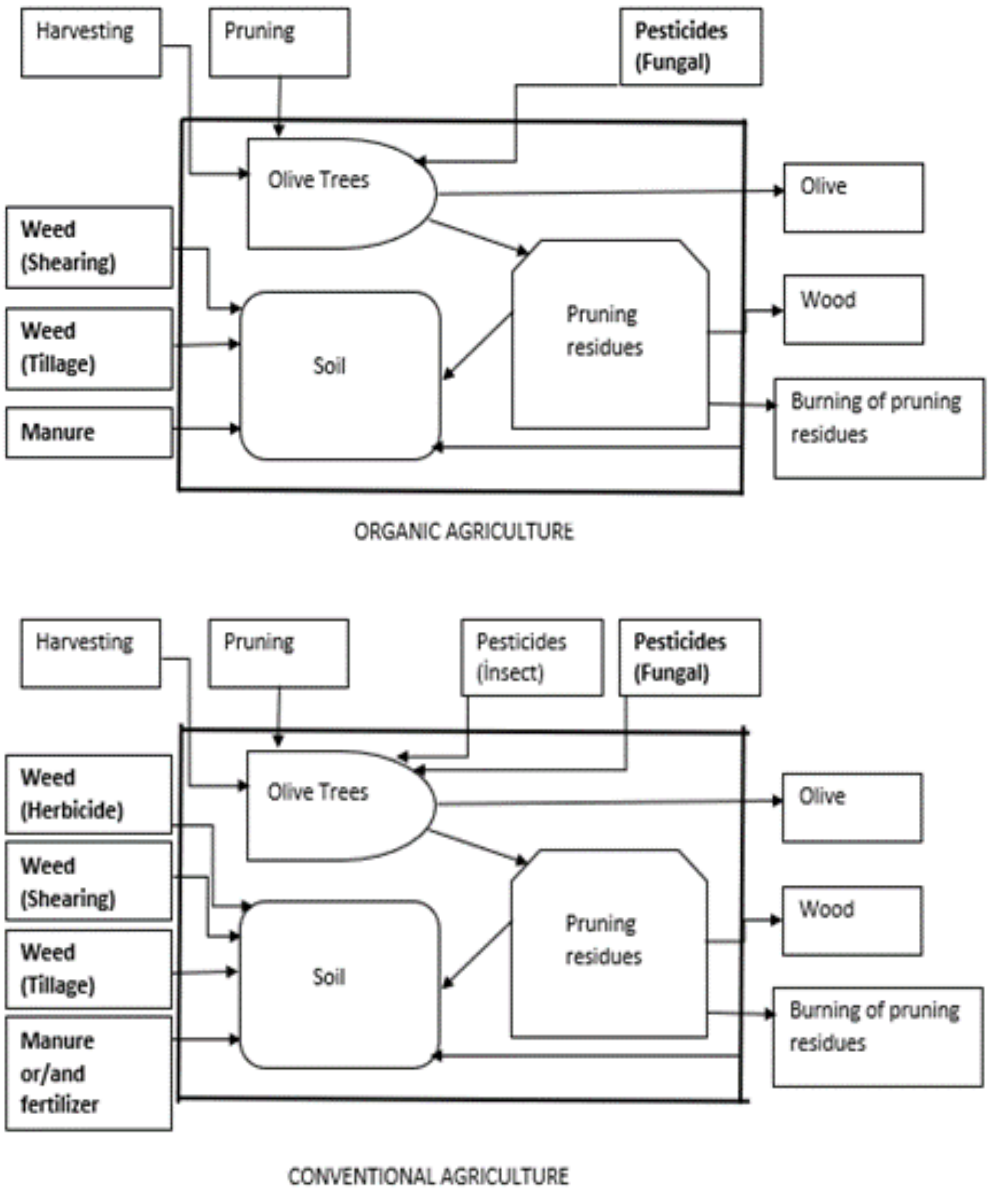

Fig. 2. System boundaries of organic and conventional olive groves. (Applications written in bold are the most frequently used applications.)

The data for the years 2015 and 2016 used in this study were taken from the project data titled 'Determination of Biodiversity Friendly Agricultural Activities in Olive Groves in Kaz Mountains'-.To be able to properly represent the production metods of the local region, GIS methods were applied. First by using ArcGIS, organic olive production sites with a size of 6 ha and above were selected and the conventional farms with similar topographic features were later included to the study [19]. In two subsequent years (2015 and 2016), face-to-face interviews were organized. In 2015, farmers from 27 organic parcels and 37 conventional parcels participated while in 2016, farmers from 24 organic parcels and 32 conventional parcels participated. The farmers were asked of their production methods, tools, inputs, and outputs throughout these two growing seasons.

The farmers were evaluated in two categories in the study: (1) Producers who carry out organic certified olive growing activities and those who have adopted organic production although they do not have a certificate, (2) Conventional producers. The farms were monitored regularly for biodiversity studies and pesticide and herbicide analyses were carried out at the end of the project. Farmers who do not follow strictly organic production protocols were removed from the organic farmers group.

2.3 Energy Efficiency in Agricultural System

Providing a global view of the efficiency of the farm process, energy analysis is an ideal method for addressing agriculture in a sustainable way [3]. To obtain the farm inputs, all the energy spent from the extraction of raw materials to the final product is calculated. This analysis also shows the socio-economic aspects of the agricultural process, as energy from fossil fuels can in some cases be replaced by human labor. The equation of energy efficiency is expressed as [3]:

$$EE(\frac{MJ}{MJ}) = \frac{\text{product energy content } (\frac{MJ}{ha.yıl})(\text{output})}{\text{enegy used for production } (\frac{MJ}{ha.yıl})(\text{input})} (1)$$

where EE is energy efficiency.

The energy efficiency calculation includes the energy content of the product and the comparison of the energy consumed. The main limits in the calculation of the energy efficiency method include economy-related inputs such as fossil fuels and fertilizers/manures, and labor-based energy inputs.

2.3.1 Energy input calculations

Energy in agricultural systems is generally examined under two main categories: direct and indirect energy use. Direct energy includes the use of electricity, fuel, oil, coal, petroleum products, natural gas, biomass, etc., which are related to the fuel use. Indirect energy, on the other hand, is the energy required for human and animal labor, agricultural implements, fertilizers/manures, pesticides, irrigation, and seed production [20]. Table 1 shows the direct and indirect energy sources included in this study.

Table 1 The Direct and Indirect Energy Sources and Related References Included in This Study

Direct Energy Sources	Indirect Energy Sources
Fuel use for the tractor [3]	Fertilizer and manure production [3]
Fuel use for chainsaw [3]	Tractor production, maintenance, and repair [3]
	Human labor [20]
	Animal labor [20]

The direct energy sources were limited to the use of fuel for the tractor and chainsaw as shown in Table 2. The engine power of agricultural implements (tractor and chainsaw), given in horsepower (HP), were converted to MJ and an additional 23% value was added for the extraction, processing, transportation and refining of final products and crude oil [3]. Indirect energy sources were listed as fertilizer/manure production, tractor production, maintenance and repair, animal, and human labor (Table 2).

The energy content of sheep and goat manure was calculated as 15.4 kcal/kg and the energy content of chicken manure was as 1.033MJ/kg with the renewable energy (grass for sheep and goats) found in the feed used by animals being included [3, 21]. The energy retained in chemical fertilizers were 47.1 MJ/kg chemical-N, 15.8 MJ/kg P2O5 and 9.3 MJ/kg K2O [3].

While calculating the amount of energy arising from the production, maintenance and repair of the tractor, the power of the tractor is converted into the mass of the tractor and the energy amount corresponding to the mass of the tractors is taken as 144 MJ/kg. When calculating the amount of machinery needed for a particular operation (kg/ha/year), the mass amount corresponding to the tractor's power (kg) is multiplied by the tractor's operation time (h/ha/year) and divided by the life of the machine (h) [3].

Table 2 shows the amount of mass corresponding to the power of the tractor and the lifetimes of the machines to calculate the amount of machine needed for a particular operation.

Table 2 The Power, Working Capacity, Weight, and Life of Tractors [22]

Tractors	Weight (kg)	Life (year)	Working time	Usage (hour/year)	Life (hour)
Tractor 0-29kW (0-40 hp)	1900	12	Hour	500	6000
Tractor 30-64kW (41-87 hp)	3300	12	Hour	600	7200
Tractor 65-94kW (88-128 hp)	5300	12	Hour	600	7200
Tractor 95-128kW (129-163 hp)	6450	12	Hour	600	7200

The energy input originating from the human labor used in the production process is expressed as follows [20]:

$$\mathbf{IE} = \frac{(\mathbf{0,268\ x\ Lf\ x\ WDlf\ x\ WHlf}) + (\mathbf{0,268\ x\ Lh\ x\ WDlh\ x\ WHlh})}{\mathbf{IA}} \quad (\mathbf{2})$$

where IE is labor energy (MJ/ha/year); Lf, Lh, family labor and hired labor (person); number of days worked (days/year) for WDlf, WDlh, family workforce and hired workforce; daily working time (hr./day) for WHlf, WHlh, family workforce and hired workforce; IA is the area worked (ha)

To calculate animal labor, following coefficients were used for the fieldwork; for horse use power was 0.50 kW and time utilization coefficient was 71% while for ox use the power was 0.40 kW and time utilization coefficient was 70% [20]. In our study area main animal labor was carried through horses.

2.3.2 Energy output calculations

Energy output was calculated by multiplying the yield (kg/ha/year) with the energy content of the olive (MJ/kg) where the energy content of 1 kg of olives was taken as 7.1 MJ [3].

3. RESULTS

3.1 The Major Differences Between Organic and Conventional Olive Production

The production method of conventional and organic olive groves had many similarities as well as differences. Within the scope of the study, one-on-one interviews were conducted with 37 conventional producers and 27 organic producers in 2015, and 32 conventional producers and 24 organic producers in 2016. Table 3 summarizes the major steps of olive production. Organic farmers mostly used manure or certified organic fertilizers whereas conventional farmers applied 15-15-15 NPK or 20-20-0 NP fertilizers intensively. In addition, conventional producers also applied ammonium sulfate fertilizer, 20-20-20 NPK fertilizer, manure, smart manure, organic manure, triple super phosphate, or potassium sulfate fertilizers. For disease control, both conventional and organic farmers used bordeaux mixture, whereas conventional farmers also used fly traps with pesticides in addition to leaf fertilizer, pesticides for olive moth and/or black scale. Regardless of organic or conventional, none of the farmers irrigated their olive groves.

Table 3 Comparison of Organic vs. Conventional Olive Production Steps in 2015 and 2016.

Year	2015				2016			
Application	Organic		Conventional		Organic		Conventional	
Fertilizer Application	Yes	No	Yes	No	Yes	No	Yes	No
	9	18	11	13	31	1	36	1
Only Manure	9		3		11		3	
Only Synthetic Fertilizer	0		31		0		25	
Both Manure and Synthetic Fertilizer	0		2		0		3	
Pest / Disease Control	Yes	No	Yes	No	Yes	No	Yes	No
	7	20	6	18	8	24	9	28
Use of Bordeaux Mixture and/or Certified Organic Pesticides	7		6		6		2	
Pesticide Use	0		1		0		1	
Bordeaux Mixture and Pesticide Use	0		2		0		5	
Weed Control	Yes	No	Yes	No	Yes	No	Yes	No
	21	6	9	15	24	8	37	0
Only Plowing	13		8		4		4	
Only Mowing	5		16		3		7	
Both Plowing and Mowing	3		3		2		3	
Herbicide Application	0		7		0		10	
Mowing and Herbicide Application	0		3		0		0	
Plowing Process	Yes	No	Yes	No	Yes	No	Yes	No
	16	11	14	10	16	16	11	26
with Tractor	7		3		8		10	
with Horse	5		3		3		3	
with both Horse and Tractor	4		5		3		3	
Pruning	Yes	No	Yes	No	Yes	No	Yes	No
	24	3	15	9	27	5	37	0

3.2 Comparing the Energy Efficiency of Organic vs. Conventional Production

We compared the conventional and organic farming practices, direct energy use (direct energy input from fuel use for tractors and chainsaws) and indirect energy use (from fertilizer/manure production, tractor production, maintenance and repair, human labor, and animal labor) for the years 2015 and 2016. (Table 4). Also, the energy efficiency of organic and conventional farming practices was compared (Table 5). Mann-Whitney U Test, a non-parametric test used for non-normal distributions was applied using the software SPSS. In both years, there was a significant difference between organic and conventional farming in terms of energy use ($p < 0.0001$) (Table 4). Organic farming needed less energy input due to using manure, a by-product of local animal husbandry, whereas conventional farming used synthetic and industrial fertilizer which required more energy input due to the production

prosess (Table 4). Fig. 3 and 4 shows individual farmers' energy input where difference between fertilizer input can clearly be seen. There was no significant difference between the direct energy inputs due to the use of fuel for tractors, chainsaws; indirect energy inputs from tractor production; maintenance and repair; human labor indirect energy inputs; and indirect energy inputs arising from animal labor with 95% confidence ($p > 0.05$) (Table 4).

Total energy use in 2015 and 2016 was significantly different between the two groups (Table 4). The total energy use of conventional agricultural practices was higher due to the high indirect energy input from the production of synthetic chemical fertilizers.

Table 4 Comparison of Energy Use Between Organic vs. Conventional Tests (** indicates statistical significance according to Mann-Whitney non-parametric U Test)

		Mean Energy (MJ/ha/yr)			Mean Energy (MJ/ha/yr)		
		Year 2015			Year 2016		
		Conv.	Org.	p-value	Conv.	Org.	p-value
		N = 37	N = 27		N = 32	N = 24	
Direct Energy	Fuel Use (Tractor)	380.38	561.55	0.231	446.56	764.16	0.914
	Fuel Use (Chainsaw)	381.84	266.44	0.086	381.47	337.28	0.578
	Total Direct Energy Use	762.22	828.00	0.940	828.03	1101.44	0.491
Indirect Energy	**Fertilizer/ Manure Production****	3164.41	367.19	< **0.0001**	4047.5	2499.32	< **0.0001**
	Tractor Production, Maintenance, Repair	134.41	200.92	0.219	125	269.12	0.957
	Human Labor	183.78	215.92	0.145	125.19	130.16	0.803
	Animal Labor	8.68	16.95	0.262	21.6	26.09	0.585
	Total Indirect Energy Use**	3491.28	800.99	< **0.0001**	4319.29	2924.69	< **0.0001**
Total Energy	**Total Energy Use****	4253.49	1628.99	< **0.0001**	5147.32	4026.13	< **0.0001**

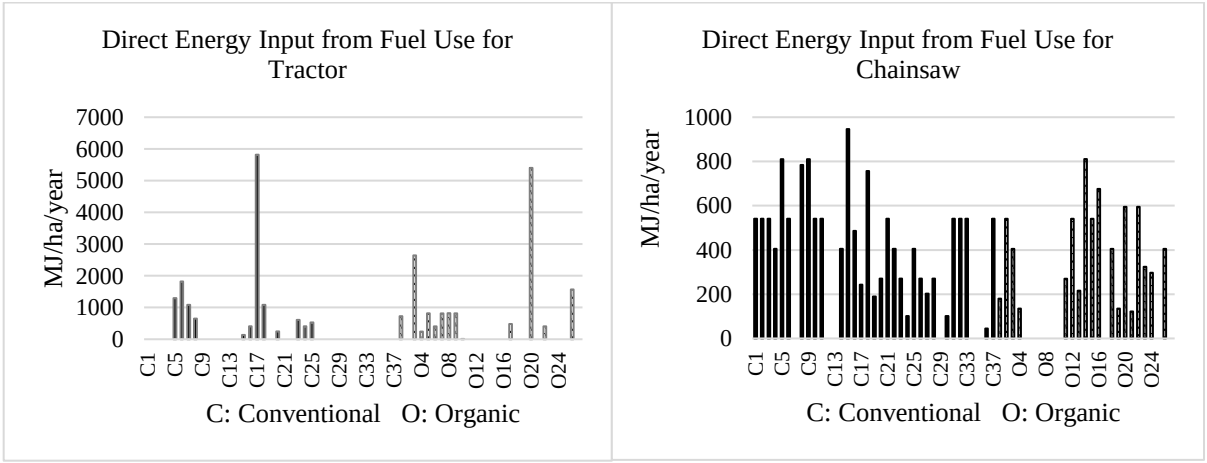

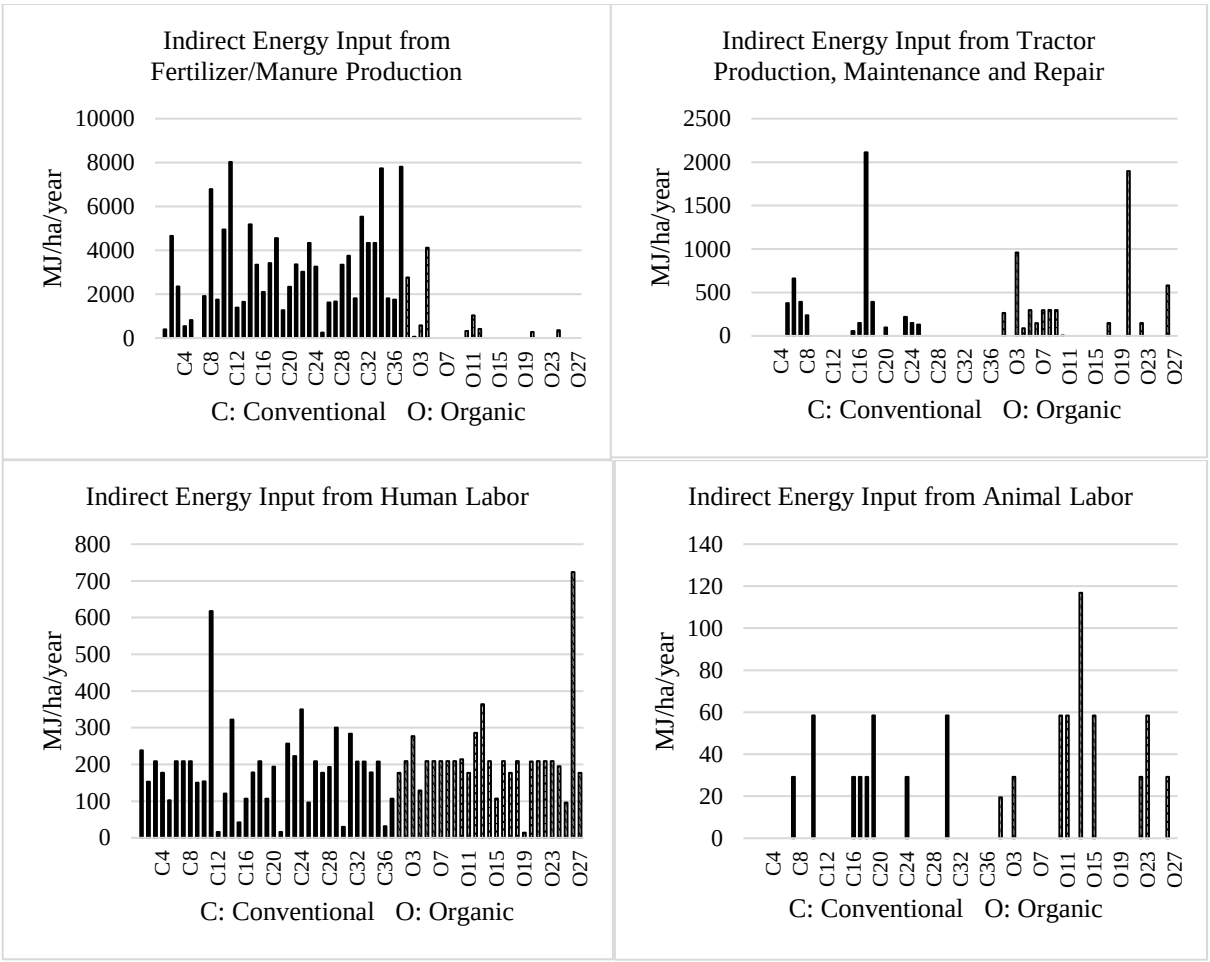

Fig. 1. Energy usage of producers in 2015

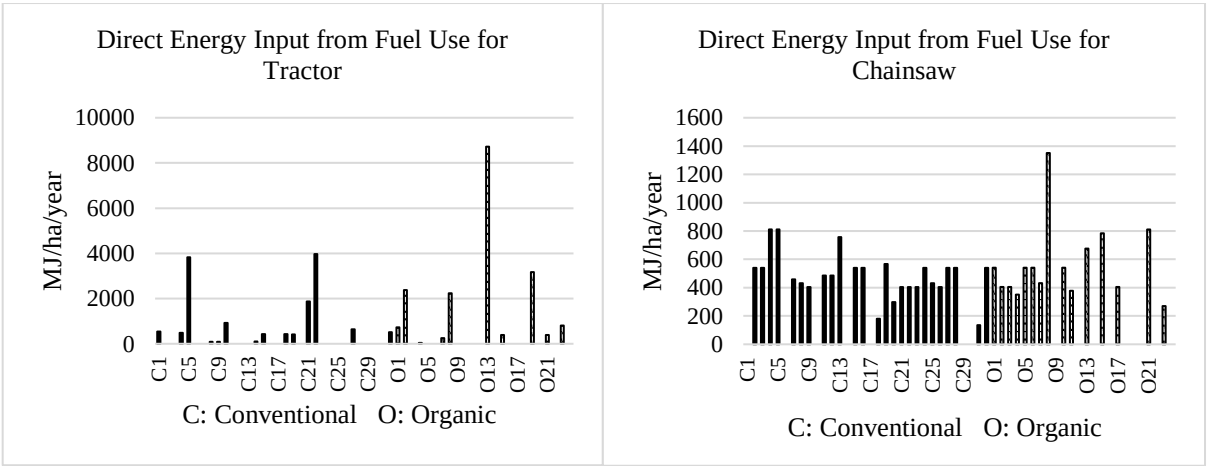

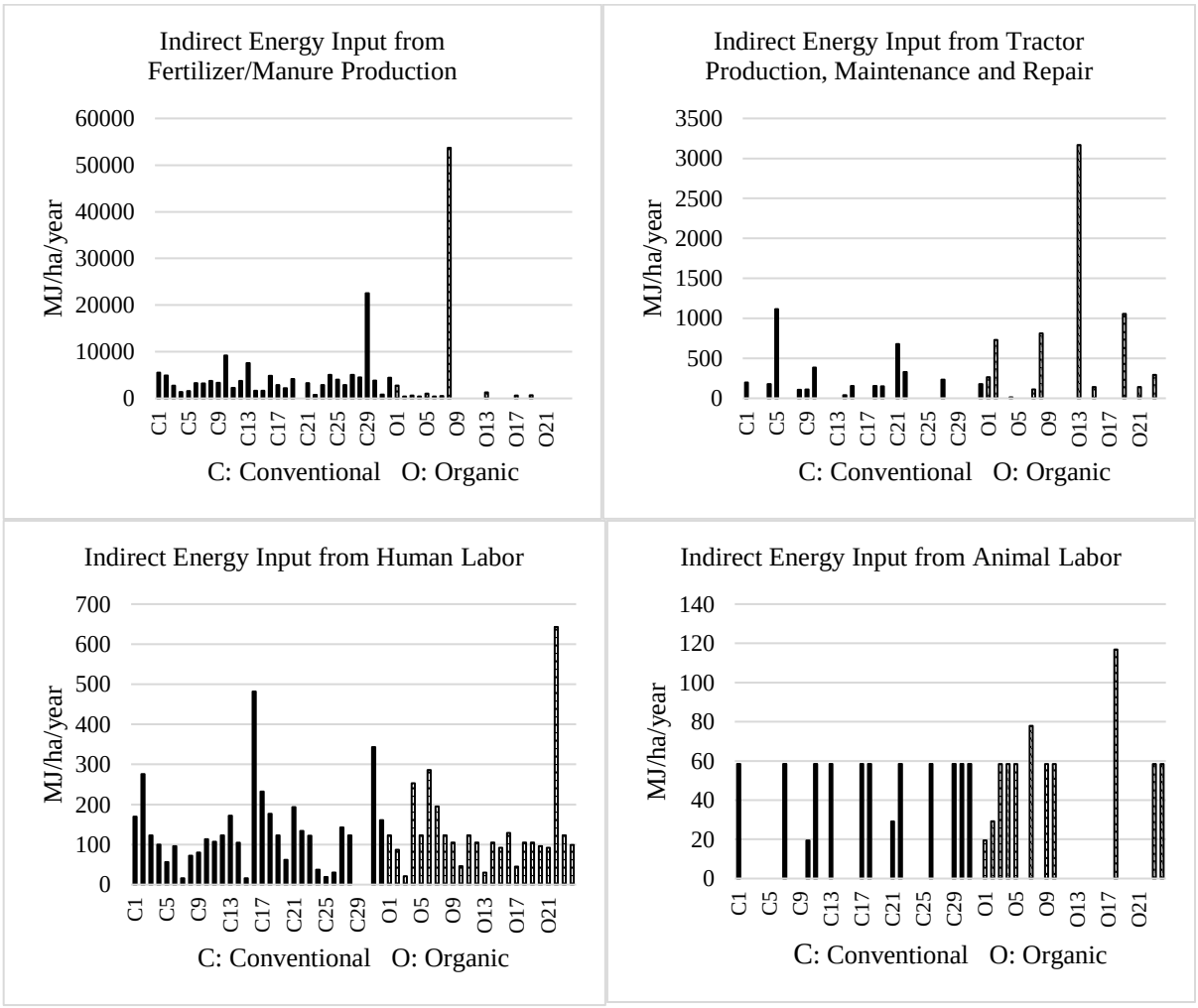

Fig. 2. Energy Use of Producers in 2016

3.2.1 Comparison of Energy Efficiency

To compare energy efficiency of organic and conventional farming Mann-Whitney U Test, a non-parametric test used for non-normal distributions was applied using the software SPSS. There was statistically significant difference between the energy efficiency of conventional and organic farming practices ($p < 0.0001$) (Table 5). Organic farming practices were more energy efficient than conventional farming practices (Fig. 5 and Fig. 6). The reason is the high indirect energy input from chemical fertilizer production in conventional agricultural practices.

Table 5 Energy Efficiency Analysis Results for 2015 and 2016 (** indicates statistical significance)

	Conventional	Organic	p-value
Mean Energy Efficiency 2015**	25.76	180.23	< **0.0001**
Mean Energy Efficiency 2016 **	24.56	220.63	< **0.0001**

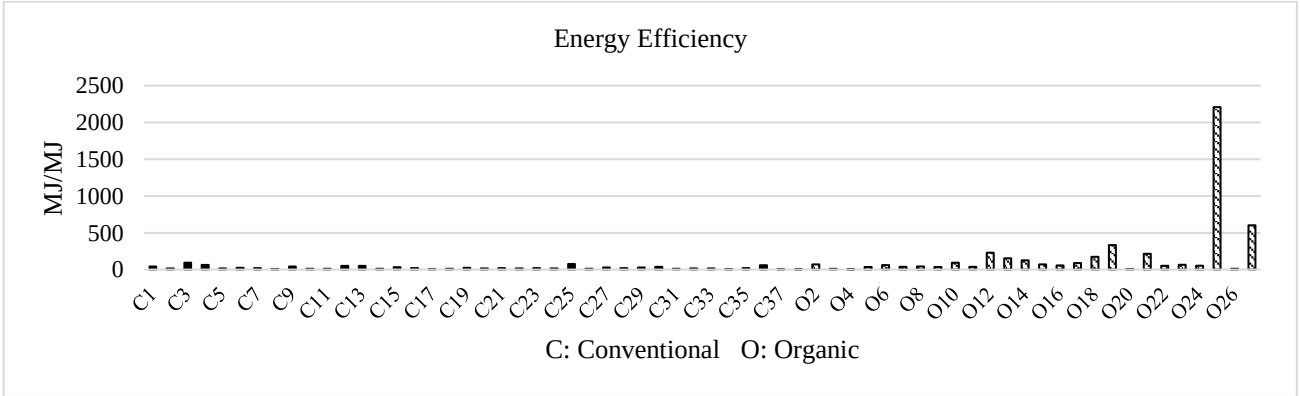

Fig. 5. Energy Efficiency of Producers in 2015

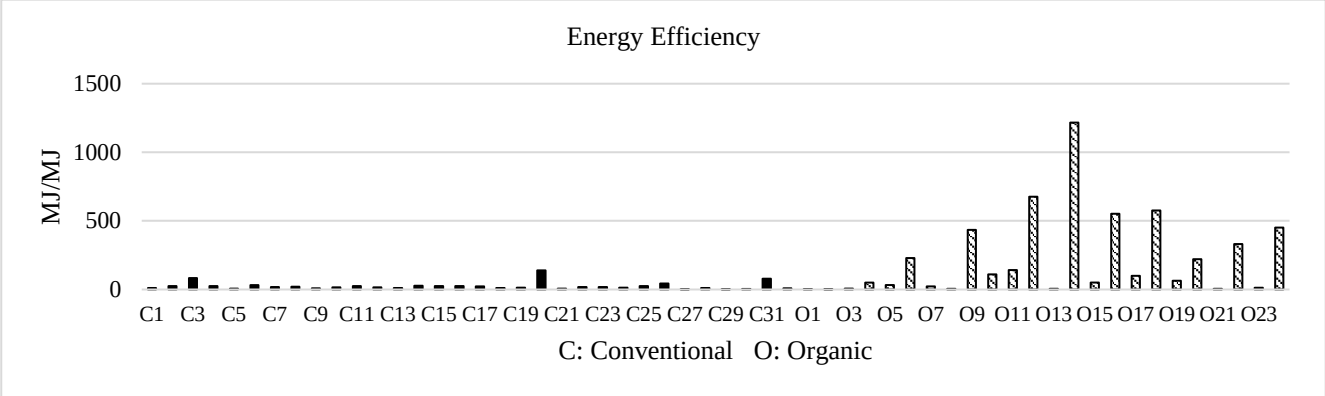

Fig. 6. Energy Efficiency of Producers in 2016

3.3 Comparison of Yield Between Conventional and Organic Olive Production

Biennial bearing is observed in olive trees of Çanakale region, which means trees have full production in one year, and only a few olives in the next year. Therefore comparing yield requires collecting data for two subsequent years. For this part of the study only farmers providing data for both of the years included. 36 producers in conventional and 13 in organic producers provided information for both years, and their data were used to compare olive yield (Fig. 7). Data did not follow a normal distribution therefore a non-parametric Mann-Whitney U Test were carried out using SPSS. The results indicate that the amount of yield changed from farmer to farmer yet there was no statistically significant difference between two farming methods (Mann-Whitney U Test, $p > 0.05$, NConventional = 36, NOrganic = 13) (Fig. 7, Table 6). This result shows that yield does not differ between the farming type.

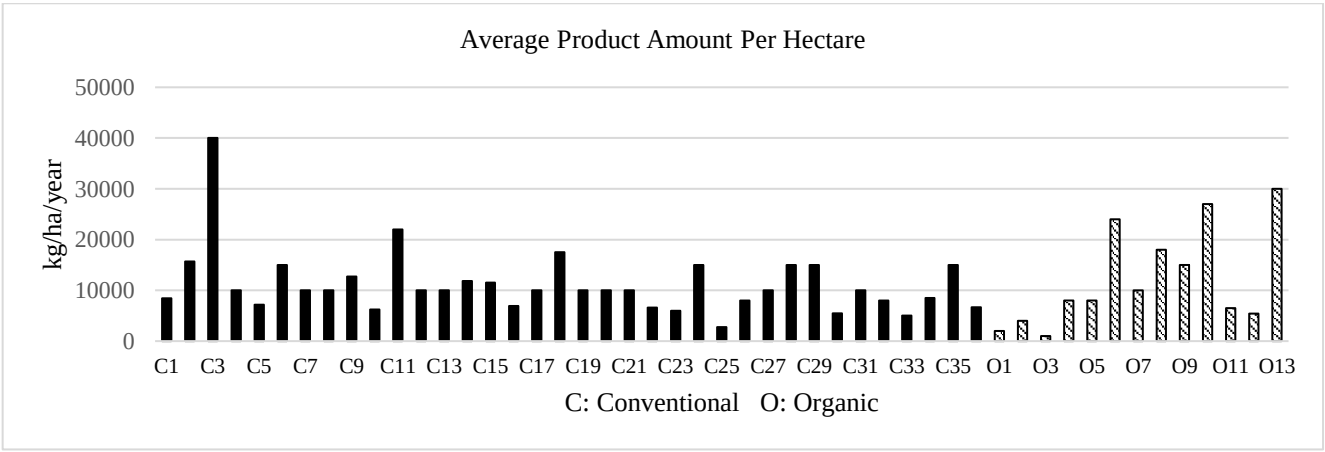

Fig. 7. Average of Production Amounts of Producers in 2015 and 2016

Table 6 Comparison of the Yield Between Conventional and Organic Farming (average yield of two subsequent years)

2015-2016					
	Application Type	Sample Size	Average (kg/ha/year)	Applied Test	Significance Value (p)
Average product quantities	Conventional	36	11,171.46	Mann-Whitney U Test (non-parametric test)	0.673
	Organic	13	13,455.38		

3.4 The Relationship Between the Yield and Energy Input

A multiple regression analysis was performed to determine if there were a relationship between the yield, the amount of fertilizer, total energy use and presence of plowing. Amount of fertilizer or total energy use did not affect the crop amount ($p > 0.05$) (Table 7). There was no significant relationship between the increase in energy use and the amount of fertilizer and the yield. On the contrary, as the amount of fertilizer, and/or the number of processes increased energy efficiency decreased yet yield did not change. For instance, farmers who do tillage using tractors had lower energy efficiency both because of direct fuel consumption and because of indirect effects such as tractor producer, maintenance, and repair, whereas farmers managed weeds by mowing had lower energy use and very similar yield.

Table 7 The Relationship Between Crop Amounts and Fertilizer Amount, Total Energy Use and Tillage

	Number of Samples	Adjusted R^2	Significance value (ANOVA test) (p)	Significance Value (p)
Yield	49	0,038	0,196	
Fertilizer/manure Amount				0,436
Total energy input				0,633
Presence of Plowing				0,095

No significant relationship was found between energy use and yield, and it was concluded that it would be possible to produce similar yield with less energy input. If energy efficiency is improved, the technical performance of agricultural systems can be increased and negative impacts on the environment can be reduced.

4. DISCUSSION AND RECOMMENDATIONS

This study compared two types of olive groves in terms of energy efficiency, and yield. The yield did not differ between two farming types, however conventional olive farms proved to be less energy efficient. The reason was mainly due to the use of synthetic fertilizers. In the study area, organic farmers preferred to use local products (i.e., locally produced manure, a by-product of local animal husbandry), as a result the energy need for growing olives were lower, while producing similar yield. Many studies find similar results to ours, for example in a study conducted by Dessane (2003) in Greece, organic olive groves were twice as energy efficient as conventional olive groves [3]. Guzman and Alonso's (2008) study in Spain revealed that organic olive cultivation has higher non-renewable energy efficiency compared to conventional olive cultivation [11]. Kavargiris et al. (2009) in their study in Greece determined that organic agriculture had a lower energy input and was more energy efficient than conventional agriculture, and therefore it was more economical [8].

This study proved that the most energy input was due to the fertilizer production and fuel use for the tractor. The energy input can considerably be reduced by decreasing the use of synthetic fertilizers. Also decreasing the use of tractor by mowing instead of plowing and increasing the use of animal labor can be given as recommendations to decrease energy input. Also, the use of renewable energy sources instead of non-renewable energy sources may be the most appropriate management method for increasing energy efficiency. One recommendation can be solarization [23], which not only decreases weed biomass but also helps increasing soluble nutrients in soil, which in turn decreases the need for fertilization [24]. However, this method can only be applied in hot regions, and it might have additional environmental effects due to the use and production of plastic, a non-renewable source. By adding a certain amount of bioethanol to the fuel, the consumption of petroleum products and air pollution can also be reduced. But there are legal issues and problems with biomaterial production. Biodiesel, which is obtained by adding methyl alcohol to oils, is a more environmentally friendly and more advantageous energy source than diesel and gasoline. Biogas is a more environmentally friendly energy source than gasoline and diesel, which is formed because of anaerobic fermentation of organic wastes. In addition, the wastes released because of anaerobic fermentation can be used as fertilizer since they have nutritive properties [23].

This study shows that by making small adjustments in farming, such as using manure instead of syntetic fertilizers, or decreasing the use of tractor and plowing it is possible to have significant impacts on energy efficiency while obtaining same amont of yield. By improving energy efficiency, the technical performance of agricultural systems can be increased and their negative impact on the environment can be reduced.

Acknowledgments
The authors gratefully acknowledge the TUBITAK for the financial support (Project No: TOVAG 213O147).

REFERENCES

[1] A. Loumou and C. Giourga, Olive groves: "The life and identity of the Mediterranean", *Agriculture and Human Values*, Vol. 20, pp. 87-95, 2002.

[2] M. Romero-Gamez, J. Castro-Rotriguez, E. M. Suarez-Rey, Optimization of olive growing practices in Spain from a life cycle assessment perspective, *Journal of Cleaner Production*, Vol. 149, pp. 25-37, 2017.

[3] D. Dessane, Energy Efficiency and Life Cycle Analysis of Organic and Conventional Olive Groves, Wageningen University, Plant Sciences, Ecological Agriculture Master of Science, Crete, pp. 102, 2003.

[4] Direk, M. (2017) Tarımda Enerji Kullanımı ve Verimliliği. http://www.tarimturk.com.tr/yazar-tarImda-enerji-kullanImI-ve-verimliligi-19.html Accessed on June 2020.

[5] Öztürk, H. H. (2006) Tarımda Yenilenebilir Enerji Kaynaklarının Kullanımı. http://www.emo.org.tr/ekler/85e48a43c7f63ac_ek.pdf Accessed on June 2020.

[6] Beyaz, A., Onurbaş Avcıoglu, A. Dayıoğlu, M.A., & Türker, U. (2016) Tarımsal Üretimde Enerji Verimliliğinin Planlanması ve Sağlanması. http://www.yegm.gov.tr/verimlilik/sunum2017/8.Bildiriler/Tar%C4%B1msal%20%C3%9Cretimde%20Enerji%20Verimlili%C4%9Finin%20Planlanmas%C4%B1%20Ve%20Sa%C4%9Flanmas%C4%B1.pdf Accessed on June 2020.

[7] E. T. Taxidis, G. C. Menexes, A. P. Mamolos, C. A. Tsatsarelis, C. D. Anagnostopoulos, K. L. Kalburtji,

Comparing organic and conventional olive groves relative to energy use and greenhouse gas emissions associated with the cultivation of two varieties, *Applied Energy*, Vol. 149, pp. 117-124, 2015.
[8] S. E. Kavargiris, A. P. Mamolos, C. A. Tsatsarelis, A. E. Nikolaidou, & K. L. Kalburtji, Energy resources' utilization in organic and conventional vineyards: Energy flow, greenhouse gas emissions and biofuel production, *Biomass and Bioenergy*, Vol. 33, pp. 1239-1250, 2009.
[9] M. Pergola, M. Favia, A. M. Palese, B. Perretti, C. Xiloyannis, G. Celano, Alternative management for olive orchards grown in semi-arid environments: An energy, economic and environmental analysis, *Scientia Horticulturae*, Vol. 162, pp. 380- 386, 2013.
[10] B. Gennaro, B. Notarnicola, & L. Roselli, G. Tassielli, Innovative olive growing models: An environmental and economic assessment, *Journal of Cleaner Production*, Vol. 28, pp. 70-80, 2012.
[11] G. I. Guzman and A. M. Alonso, A comparison of energy use in conventional and organic olive oil production in Spain, *Agricultural Systems*, Vol. 98, pp. 167-176, 2008.
[12] G. Todde, L. Murgia, P. A. Deligios, R. Hogan, I. Carrelo, M. Moreira, A. Pazzona, L. Ledda, L. Narvarte, Energy and environmental performances of hybrid photovoltaic irrigation systems in Mediterranean intensive and super intensive olive orchards, *Science of The Total Environment*, Vol. 651, pp. 2514-2523, 2019.
[13] (2015) 2014 Yılı Zeytin ve Zeytinyağı Raporu. T.C. Gümrük ve Ticaret Bakanlığı Kooperatifçilik Genel Müdürlüğü, Türkiye.
[14] Anonymous, (2017) Türkiye'de Zeytincilik. https://zeytindostu.org.tr/zeytin/turkiyede-zeytincilik Accessed on June 2019.
[15] R. Ilgar, Çanakkale ilinde tarımda sürdürülebilirlik ve organik tarım, *Doğu Coğrafya Dergisi*, Vol. 22, pp. 159-178, 2017.
[16] N. Koca, Çanakkale'de zeytin yetiştiriciliğinin coğrafi esasları, *Marmara Coğrafya Dergisi*, Vol. 9, pp. 119-137, 2004.
[17] G. Yılmaz, İda dağı (kazdağları) nın sağlık turizmi çerçevesinde incelenmesi, *International Anatolia Academic Online Journal Social Sciences Journal*, Vol. 4, pp. 15-35 2018.
[18] Özel, N. (1999) Kaz Dağları Orman Vejetasyonu Üzerine Fitososyolojik ve Fitoekolojik Araştırmalar. https://egearastirma.ogm.gov.tr/Yayinlar/Teknik%20B%C3%BClten/TEKN%C4%B0K%20B%C3%9CLTEN%2011%20Kaz%20Da%C4%9Flar%C4%B1%20Orman%20Vejetasyonu%20%C3%9Czerine%20Fitososyolojik%20Ve%20Fitoekolojik%20Ara%C5%9Ft%C4%B1rmalar.pdf Accessed on June 2020.
[19] (2017) 2015-2016 Kaz Dağları'ndaki Zeytinliklerde Biyolojik Çeşitlilik Dostu Tarım Faaliyetlerinin Belirlenmesi (TÜBİTAK 1001 Proje no. 213O147) Sonuç Raporu, Kaz Dağları.
[20] Öztürk, H. H., *Bitkisel üretimde enerji yönetimi*, Hasad yayıncılık ve Ümraniye, 2011.
[21] M. D. Heidari, M. Omid, & A. Akram, Energy efficiency and econometric analysis of broiler production farms, *Energy*, Vol. 36, pp. 6636-6541, 2011.
[22] Nemecek, T. and Kägi, T. (2007) Life Cycle Inventories of Swiss and European Agricultural Production Systems. https://db.ecoinvent.org/reports/15_Agriculture.pdf Accessed on October 2019.
[23] A. G. Bayrakcı and G. Koçar, Utilization of renewable energies in Turkey's agriculture, *Renewable and Sustainable Energy Reviews*, Vol. 16, pp. 618-633, 2011.
[24] Kitiş, Y. E. (2012) Solarizasyon Nedir? Nasıl Uygulanır? http://solarizasyon.blogspot.com/2012/10/tarm-gunlugu-dergisi-say-10.html Accessed on October 2020.

Founded in 2016, our association is open to everyone who is interested in energy and devoted to sustainability.

ERCIYES ENERGY ASSOCIATION